

Marquette University

e-Publications@Marquette

Master's Theses (2009 -)

Dissertations, Theses, and Professional
Projects

NMR and Computational Studies of NAD(P)(H) Cofactor Binding

Junghwa Kim
Marquette University

Follow this and additional works at: https://epublications.marquette.edu/theses_open



Part of the [Chemistry Commons](#)

Recommended Citation

Kim, Junghwa, "NMR and Computational Studies of NAD(P)(H) Cofactor Binding" (2011). *Master's Theses (2009 -)*. 117.

https://epublications.marquette.edu/theses_open/117

NMR AND COMPUTATIONAL STUDIES OF NAD(P)(H) COFACTOR BINDING

by

JUNGHWA KIM

A Thesis submitted to the Faculty of the Graduate School,
Marquette University,
in Partial Fulfillment of the Requirements for
the Degree of Master of Science

Milwaukee, Wisconsin
December 2011

ABSTRACT

NMR AND COMPUTATIONAL STUDIES OF NAD(P)(H) COFACTOR BINDING

JUNGHWA KIM, B.A.

Marquette University, 2011

Tuberculosis (TB) is one of the most dangerous diseases in a sense of spread method. According W.H.O., one third of world population has this disease and annual one of these infected people spreads 10 -15 people unintentionally. To protect human from this bacterial, the unique feature of mycobacterial TB was studied previously. The unique cell wall, peptidoglycan, has high content of DAP (diaminopimelic acid). The disruption of synthesis DAP results in cell death due to instability of cell wall. One way to inhibiting synthesis of DAP is to modify cofactor which acts with dehydrogenase. To do that the study of cofactor is necessary.

There are limitation for determination of Nitrogen and Oxygen by X-ray Crystallography. Recent research paper found several examples that Nitrogen and Oxygen of carboxamide on Nicotinamide adenosine dinucleotide (NAD(P)(H) were misplaced in X-ray crystallography. NMR is more accurate measurement on Nitrogen and Oxygen determination. For NMR studies, ^{15}N labeled cofactors are required due to a half spin property of Nitrogen. The synthesis of ^{15}N labeled cofactors, NAD(P)(H), will be addressed. Additionally, Energy, charge, NMR, resonance structures are studied with computational calculation, Gaussian 9.0 and NBO5. There are several distinctive differences between carboxamide conformation on NAD(P)(H) by Conjugation, Nitrogen, substituent, and steric hinderance effects.

Our findings will help understanding of cofactors binding enzyme. It will facilitate the drug development.

TABLE OF CONTENTS

LIST OF TABLES.....	iii
LIST OF FIGURES.....	iv
Chapter I. Dynamic and structural changes of ^{15}N labeled NAD(P)(H) with binding proteins	
1. Introduction.....	1
1.1 Rationale for Design of the Conformational Dynamics Ligand Probe.....	5
1.2 Materials and Methods.....	6
1.3 Synthesis of [^{15}N -CA]-nicotinamide.....	6
1.4 Synthesis of [^{15}N -CA]-NAD $^{+}$	8
1.5 Synthesis of [^{15}N -CA]-NADP $^{+}$	12
1.6 Synthesis of [^{15}N -CA]-NADH.....	15
1.7 Synthesis of [^{15}N -CA]-NADPH.....	17
1.8 HSQC DATA	18
1.9 Results and Discussion.....	22
1.10 Conclusion.....	23

Chapter II. Conformational analysis of NAD(P)(H) by computational methods

2. Introduction.....	24
2.1 Materials and Methods.....	28
2.2 Rotational energy of NAD(P)(H).....	31
2.3 Charges on active regions of NAD(P)(H).....	68
2.4 Resonance structures of NAD(P)(H).....	70
2.5 Spectroscopic analysis of NAD(P)(H)): Calculation of NMR chemical shift.....	79
2.6 Results and Discussion.....	81
2.7 Conclusion.....	83
BIBLIOGRAPHY	
APPENDIX.....	84

LIST OF TABLES

Table 2.3.1.....	69
Table 2.5.2.....	81

LIST OF FIGURES

Figure 1.....	2
Figure 2.....	3
Figure 3.....	4
Figure 1.3.1.....	7
Figure 1.3.2.....	8
Figure 1.4.1.....	9
Figure 1.4.2.....	10
Figure 1.4.3.....	11
Figure 1.5.1.....	13
Figure 1.5.2.....	13
Figure 1.5.3.....	14
Figure 1.6.1.....	16
Figure 1.6.2.....	17
Figure 1.7.....	18
Figure 1.8.1.....	18
Figure 1.8.2.....	19
Figure 1.8.3.....	20
Figure 1.8.4.....	20
Figure 1.8.5.....	21
Figure 1.8.6.....	21
Figure 2.1.....	25
Figure 2.2.....	26

Figure 2.3.....	27
Figure 2.4.....	28
Figure 2.1.1.....	29
Figure 2.1.2.....	30
Figure 2.1.3.....	30
Figure 2.2.1.....	32
Figure 2.2.2.....	33
Figure 2.2.3.....	34
Figure 2.2.4.....	36
Figure 2.2.5.....	37
Figure 2.2.6.....	38
Figure 2.2.7.....	40
Figure 2.2.8.....	41
Figure 2.2.9.....	42
Figure 2.2.10.....	43
Figure 2.2.11.....	44
Figure 2.2.12.....	45
Figure 2.2.13.....	46
Figure 2.2.14.....	47
Figure 2.2.15.....	48
Figure 2.2.16.....	49
Figure 2.2.17.....	50
Figure 2.2.18.....	51
Figure 2.2.19.....	52
Figure 2.2.20.....	54

Figure 2.2.21.....	55
Figure 2.2.22.....	56
Figure 2.2.23.....	57
Figure 2.2.24.....	58
Figure 2.2.25.....	59
Figure 2.2.26.....	60,61
Figure 2.2.27.....	63
Figure 2.2.28.....	63-65
Figure 2.2.29.....	66
Figure 2.2.30.....	67
Figure 2.3.1.....	68
Figure 2.4.1.....	70-72
Figure 2.4.2.....	72-74
Figure 2.4.3.....	74-76
Figure 2.4.4.....	77,78
Figure 2.5.1.....	80

Chapter I. Dynamic and structural changes of ^{15}N labeled NAD(P)(H) with binding proteins

1. Introduction

Tuberculosis (TB) is a contagious disease that is transmitted via coughing, sneezing, or other aspiration that is transferred. The most dangerous part of TB is that people can be infected with TB bacilli for years, and do not feel sick until their immune system is weakened, at which point the TB becomes “active.” Active TB bacilli in infected people can spread TB unintentionally. According to the WHO (<http://www.who.int/mediacentre/factsheets/fs104/en/>), one-third of the world’s population has TB bacillus in their body and each infected person spreads TB disease on average to 10 -15 people in a year. Treatment for TB must continue for 4-6 months, using a cocktail of drugs: isoniazid, rifampin, ethambutol, and pyrazinamide. Recently, multidrug-resistant (MDR) strains of TB have emerged. The treatment of this resistant TB strain is done using so-called second-line treatments, which are more costly and have more side effects. Therefore, the development of new and more effective anti-tuberculosis drugs is necessary¹⁻³.

The distinctive composition of the peptidoglycan cell wall of mycobacterium is target of many drugs; it has a high degree of interpeptide cross-linking, primarily through meso-Diaminopimelic acid (DAP) cross-links in addition to the DAP. DAP biosynthesis is central to the structure of the mycobacterial peptidoglycan. So, DAP syntheses (and lysine synthesis) is a potential target for killing mycobacteria, such as *Mycobacterium smegmatis* and *Mycobacteria tuberculosis*. Disruption of biosynthesis of DAP results in cell death due to instability of the peptidoglycan^{14,15}. There are three known methods for biosynthesis of DAP by mycobacteria (Fig 1). The dihydrodipicolinate reductase (DHPR, also called

dapB) gene of mycobacteria is a potentially useful target for the development of new antibiotics, specific for mycobacteria, because its inhibition can inhibit of the three parallel biosynthetic pathways for the synthesis of DAP in mycobacteria, such as BCG (*Bacterium bovis*)¹⁴, as shown in Fig. 1.

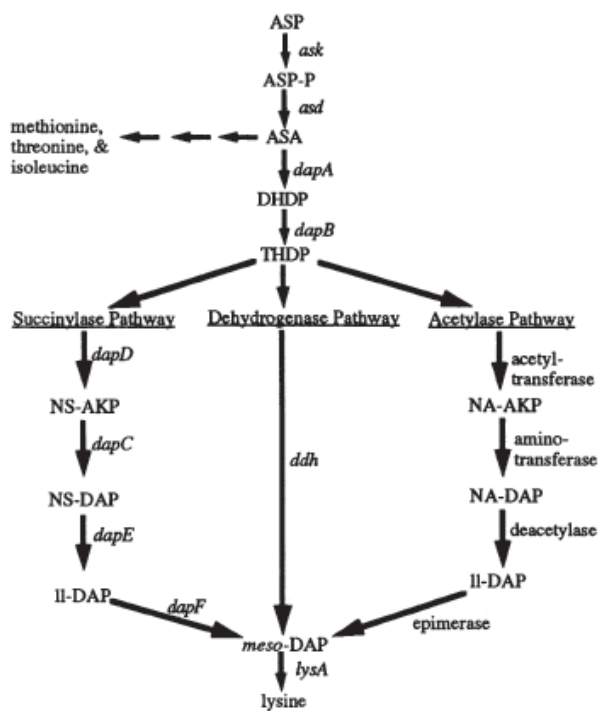


Figure 1. Three pathways for synthesis of meso-DAP and lysine. Three major pathways: Succinylase pathway, Dehydrogenase pathway, Acetylase pathway.

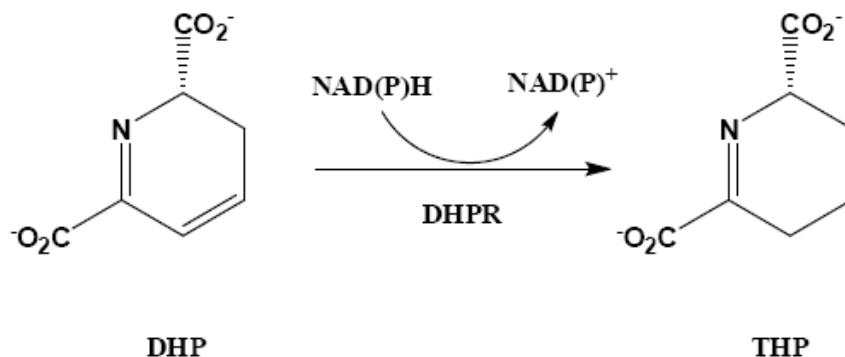


Figure 2. Reaction with Dihydrodipicolinate reductase (DHPR, also called dapB)

Figure 1 shows the pathway for synthesis of L-lysine in gram-negative bacterial and *Mycobacterium tuberculosis* (*M. TB*).

Dihydrodipicolinate reductase (DHPR, also called dapB) catalyzes the NAD(P)H dependent reduction of the carbon-carbon double bond of the α,β -unsaturated cyclic imine, dihydrodipicolinate, to form the cyclic imine, tetrahydrodipicolinate (Figure 2). Similarly, Dihydrodipicolinate reductase (DHPR), with help of a cofactor, the reduced form of Nicotinamide adenine dinucleotide phosphate (NADPH), converts dihydrodipicolinate to tetrahydrodipicolinate. Dihydrodipicolinate reductase (DHPR) is a potential drug target for treating TB⁴⁻⁶.

NADP(H) is used as the cofactor for multiple enzymes in cell wall synthesis pathways, in addition to DHPR. The mechanism and structural study of NAD(H)/NADP(H) bound to these enzymes will improve our basic understanding of an important class of enzymes, but may also help guide the development of anti-TB drugs that inhibit these enzymes. And, given the importance of the NADPH cofactor in other enzymatic redox reactions, its mechanism is of broad interest.

The mechanism and structural conformation of enzyme-bound NAD(H)/NADP(H) are studied by computational and NMR methods presented herein.

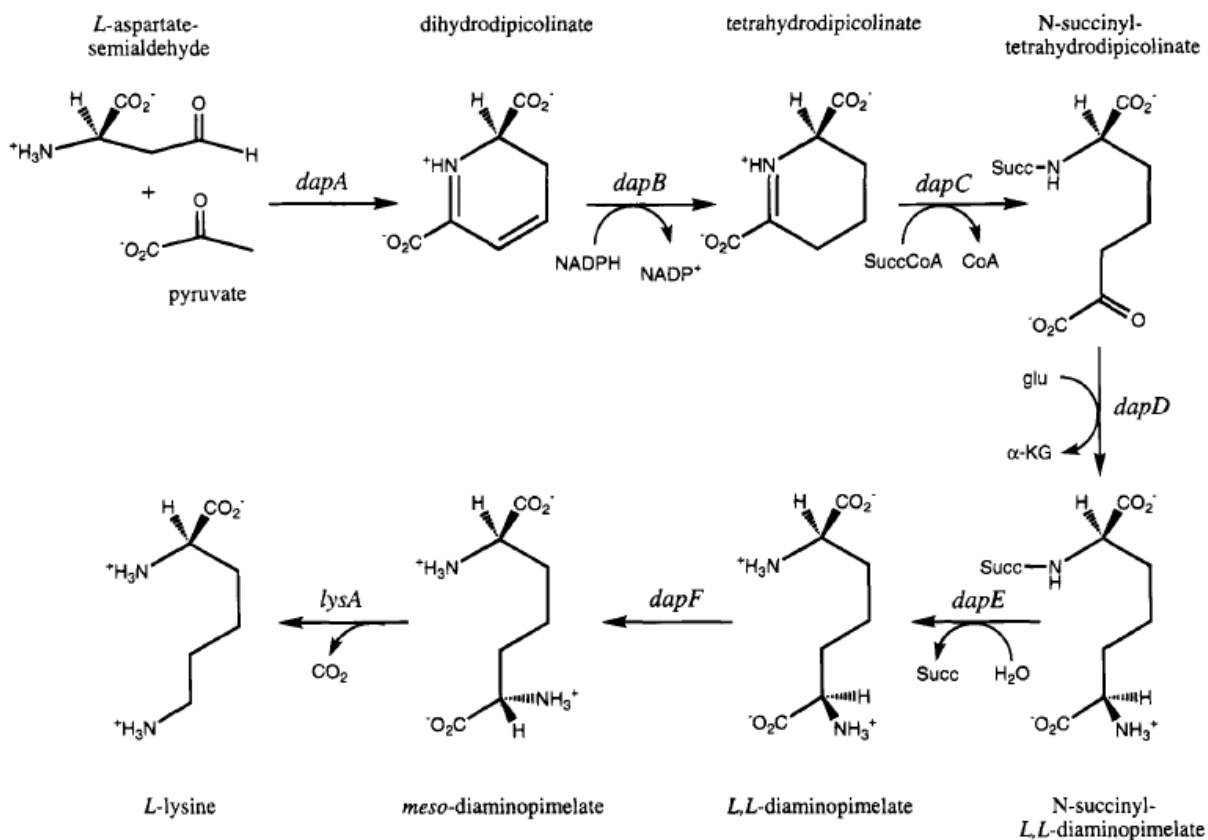


Figure 3 Lysine and meso-diaminopimelate (DAP) biosynthetic pathway in *E. coli*⁴.

1.1 Rationale for Design of Conformational Dynamics Ligand Probe

In almost all living systems, most chemical reactions need enzymes to lower activation energy and increase reaction rates. In many cases, enzymes require non-protein molecules called cofactors for their activities. Understanding in changes of conformational Enthalpy and Entropy due to interactions between substrate, cofactor, and protein is necessary to understand mechanism. An unbounded cofactor has higher entropic energy, since there are few restrictions on bond rotations. Once, a cofactor bounds to an enzyme is loses entropic energy, and enthalpy gains (ex. formation of hydrogen bonds; Van der Waals interactions) typically offset this entropic penalty. The study in Enthalpic and Entropic contribution to enzymatic reaction is now an important part of the drug design process.

The reduced or oxidized forms of nicotinamide adenine dinucleotide (NAD) and nicotinamide adenine dinucleotide phosphate (NADP), one of largest classes of cofactors, are ubiquitous in all living systems. 370 different kinds of enzymes according to *Enzyme Nomenclature*, and seventeen percent of all classified enzymes require NAD(P)(H)¹¹. The weight of importance of these enzymes is significant.

Undoubtedly, the characterization of dynamic changes in the NAD(P)(H) will improve understanding of enzymatic mechanisms in various enzymatic reactions, which reacts with NAD(P)(H).

The possible conformational studies of NAD(P)(H) are derived from the base-ribose, glycosidic orientation, folded and opened forms, and the structure of the dihydronicotinamide ring^{10,11}.

In unbounded states, the conformation of pyridine dinucleotides in solution has three different conformations, extended, folded, and hydrogen-bonded. Among those conformations, a folded conformation with the planes of the two rings stacked in parallel is the most abundant, and exchanges with the open conformation¹².

Previously the Sem lab used NMR relaxation dispersion methods to study the exchange between folded and opened conformations of free NAD(P)(H); the msec timescale conformational exchange was consistent with a proposed conformational exchange proposed by Jardetzky¹³, thereby validating our approach. The relaxation dispersion methods we use are based on Carr-Purcell-Meiboom-Gill (CPMG) based T2 measurements, which will be used to study conformational exchange rate changes that occur after coenzyme binds to protein. Such studies are based on measurements of the motional properties (reflected in T2 values) for the N-H amide bond vector; such experiments require that nitrogen be present as ¹⁵N (spin ½) rather than the naturally more abundant ¹⁴N (spin 1, and quadrupolar). So, synthesis of ¹⁵N-NAD(P)(H) is therefore, needed, to help analyze the structural and dynamic information of the NAD(P)(H) cofactor by relaxation dispersion, as well as ¹⁵N-HSQC and ¹⁵N-filtered NOESY experiments. The studies presented herein are focused on the synthesis (chemical and enzymatic) of these labeled cofactors, to enable these NMR studies.

1.2 Materials and Methods

1.3 Synthesis of [¹⁵N-CA]-nicotinamide

4.9 g KOH pellets and 60 mL deionized water were prepared in a 250 mL round bottom flask with a magnetic stir bar. After KOH pellets were dissolved completely, 1.5 g of ¹⁵N-NH₄Cl was added to this solution. Additionally, 5.01g of Nicotinoyl chloride HCl (purchased from Sigma Aldrich) was added over 10 min. pH of the solution was adjusted to 11. Solution was stirred for 2hrs, until completion of the reaction. For confirmation of [¹⁵N-CA]-nicotinamide formation, Figure 1, TLC was checked with comparison made to Isotope grade nicotinamide. Water was removed by lyphilizing. 0.72 g of 4Åmolecular sieves and 50 mL of benzene were added into a dried 250 mL round bottom flask. Dried

powder of the ^{15}N nicotinamide was transferred into the benzene solution. Reflux was performed 2-3 hours by azeotropic distillation for additional water extraction. The Hot Solution was filtered with filter paper (P8) purchased from Fischer. The solution was filtered one more time with a fine filter funnel from Kontes Williamson: ST 14/20 macroscale kit (purchased from Sigma-Aldrich). 17% of (0.589 g) [^{15}N -CA]-nicotinamide was the yield. For confirmation of ^{15}N labeled Nicotinamide, a 1-D HSQC NMR experiment was performed at low Temperature 4°C , Figure 2. This NMR spectrum shows the signal for protons attached to ^{15}N on the nicotinamide ring amide.

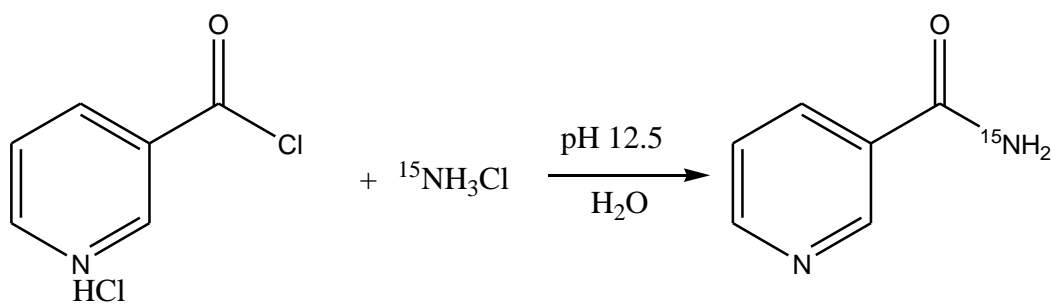


Figure 1.3.1 Chemical structure after ^{15}N labeled NH_3 is added to the Pyridine.

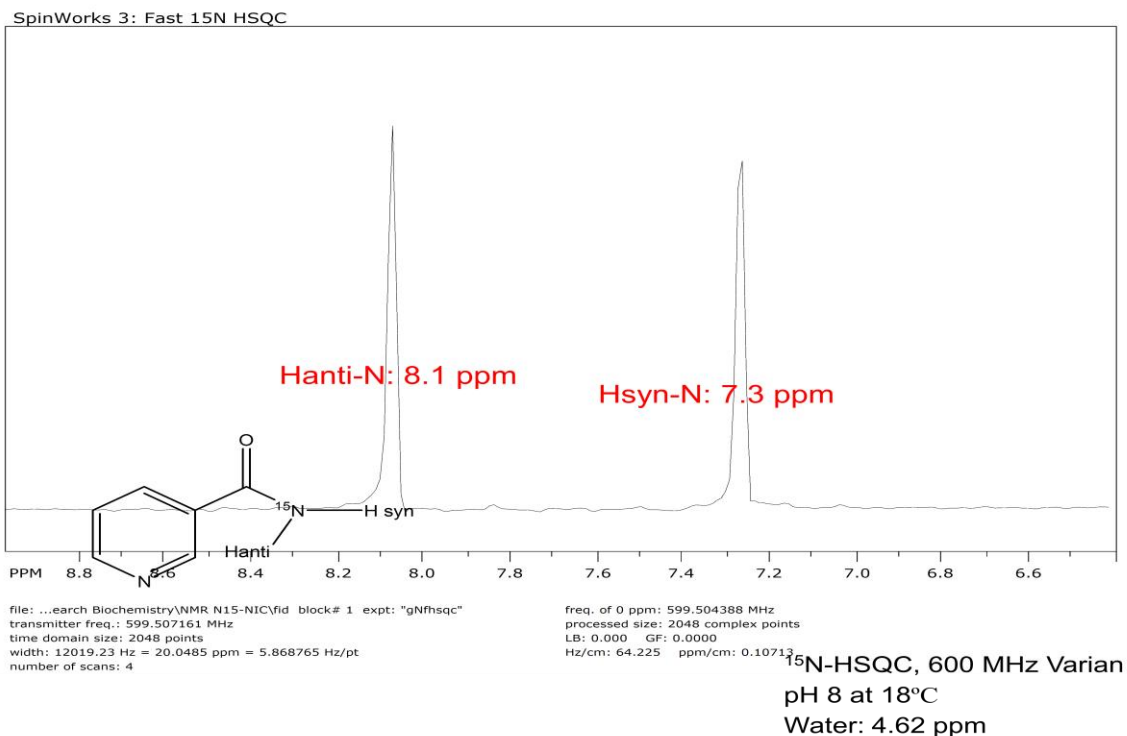


Figure 1. 3. 2. ¹⁵N-HSQC filtered 1D spectrum of ¹⁵N nicotinamide in 50mM Tris buffer, 4°C, pH 11, collected on a 600 MHz Varian NMR System. The N-H that is anti to the carbonyl (at 8.1 ppm) is more acidic, and then N-H that is syn (7.3 ppm) less acidic. Lower pH leads to loss of signal intensity due to exchange with water (4.61 ppm).

1.4 Synthesis of [¹⁵N-CA]-NAD⁺

Reaction mixture containing 5 mM NAD, 50 mM of [¹⁵N-CA]-nicotinamide, in 20ml of 50mM Tris buffer, 200 units of porcine brain NADase (purchased from Sigma-Aldrich) of 50mM Tris buffer, and 40ml of 50mM Tris buffer were prepared and pH of solution was adjusted to pH 7.3. Before incubating the above mixtures at 37°C, 1 mL of NAD⁺ and a mixture of 500 uL of NAD⁺ and 500uL of NADase were prepared separately as a control sample to confirm the full exchange of [¹⁵N-CA]-nicotinamide into NAD⁺. Control sample and the reaction mixture were started, incubating at 37°C until UV absorbance of

the control sample was recorded (figure 1.4.1), using the cyanide method⁹. 10 μ L of sample was added to 990 μ L of 1.0 M NaCN in a 1ml quartz cuvette, and 1 mL of cyanide solution was used as a blank. The UV absorbance at 340 nm decreased (20 hours) from 0.0318 to 0.0058. This confirmed Nicotinamide ring detachment from NAD⁺, by the NADase enzyme (note: in the presence of excess nicotinamide, there is simply a nicotinamide ring swap, rather than loss of nicotinamide ring).

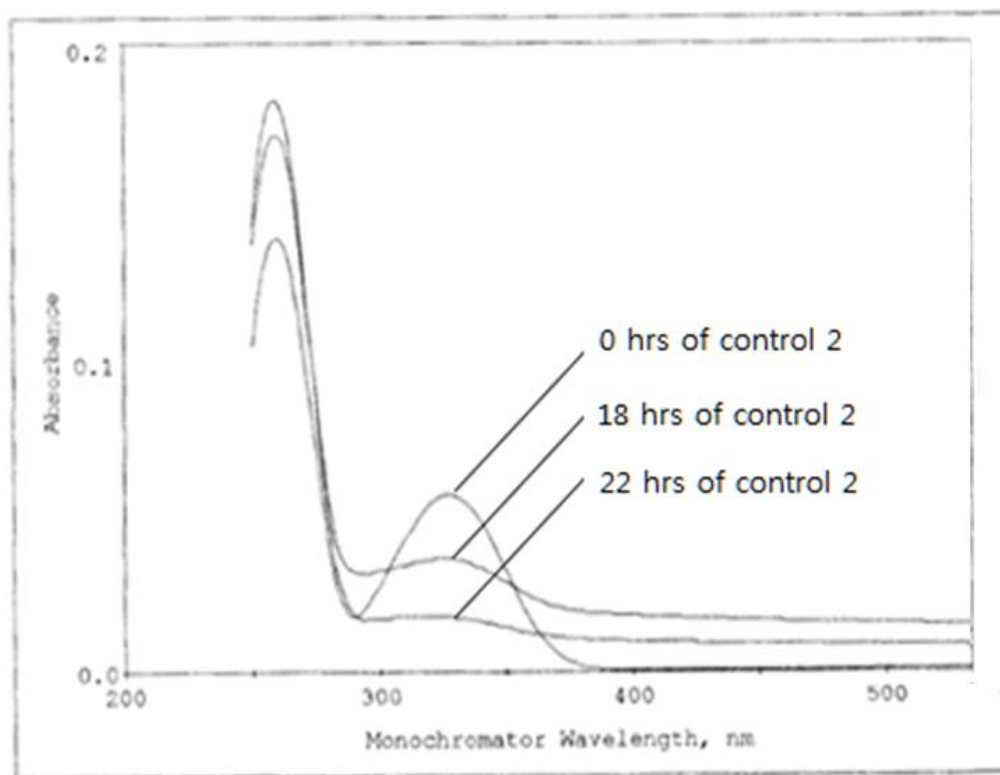


Figure 1.4.1 Control sample of a mixture of 500 μ L of NAD⁺ and 500 μ L of NADase; UV-absorbance at 340nm was decreased from 0.0318 to 0.0058, due to loss of the nicotinamide ring from NAD⁺. A is the control sample at the beginning of NADase reaction after the CN reaction. B is the control sample at the middle of NADase reaction after CN reaction. C is the control sample at the end of NADase reaction after CN reaction.

Then the mixture was heated up to 70 °C for 2 minutes to deactivate the NADase enzyme. The deactivated protein was separated by centrifuging at 4000rpm, and supernatant was collected for further purification.

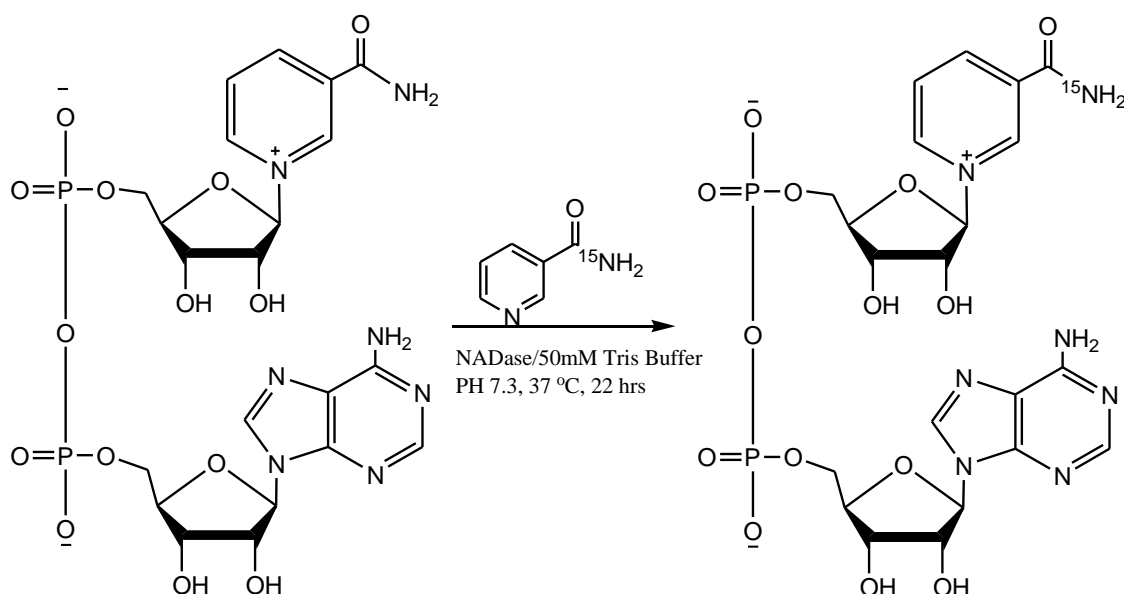


Figure 1.4.2. Synthesis of ^{15}N -NAD $^{+}$

$[^{15}\text{N-CA}]\text{-NAD}^{+}$ was further purified using a BioGel P2 gel (Bio-Rad) column with 50mM Tris buffer at pH 7.3. The product purified was analyzed with the cyanide method⁹ to detect NAD $^{+}$. To perform the assay, 10 μL of sample was added to 990 μL of 1.0 M NaCN in a 1ml quartz cuvette, and 1 mL of cyanide solution was used as a blank.

The final concentration of $[^{15}\text{N-CA}]\text{-NAD}^{+}$ was determined using an alcohol dehydrogenase enzymatic endpoint assay. To perform this assay, 10 μL of 2mM methanol, 10 μL (16 units) of yeast Alcohol Dehydrogenase (purchased from Sigma-Aldrich), and 50 μL of $[^{15}\text{N-CA}]\text{-NAD}^{+}$ were added to 930 μL of

Tris buffer at pH 7.3. UV-absorbance at 340 nm was monitored in Figure 1.4.3, and concentration calculated using a molar extinction coefficient of $6220 \text{ M}^{-1} \text{ cm}^{-1}$. The concentration of $^{15}\text{N-NAD}^+$ was calculated to be $864 \mu\text{M}$. The product was stored after either flash freezing in liquid nitrogen, or else after lyophilizing overnight.

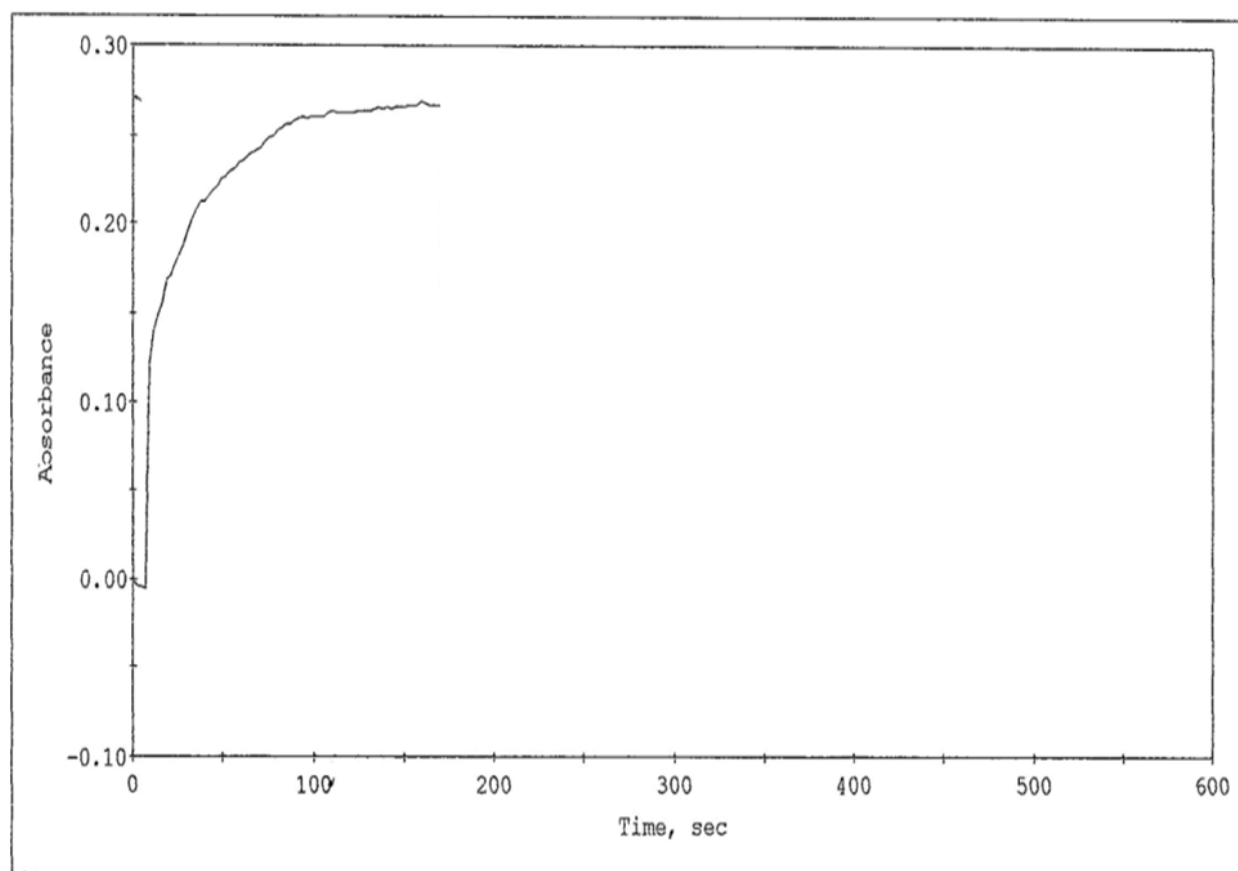


Figure 1.4.3 enzymatic end point assay to determine concentration of NAD^+ , using 10 μL of 2mM methanol, 10 μL (16 units) of yeast Alcohol Dehydrogenase (purchased from Sigma-Aldrich), and 50 μL of $^{15}\text{N-CA-NAD}^+$, added to 930 μL of Tris buffer at pH 7.3, Absorbance= 0.269, Concentration= 864 μM

The stability of $^{15}\text{N-NAD(P)}$ after several freeze-thaw cycles was determined at various pH's (2.3 - 7.3).

The concentration of coenzymes was analyzed with alcohol dehydrogenase assay after each thaw. With

50mM Tris buffer at various pH (2.3 - 7.3), the concentration of $^{15}\text{N-NAD}^+$ was constant, from 550 μM to 553 μM . However, with phosphate buffer with various concentrations (20mM to 200mM) at various pH's (2.3-7.3) the stability of the coenzyme ($^{15}\text{N-NAD}^+$) was much lower, with concentrations going from 500 μM to 0 μM — determined using the KCN method and the alcohol dehydrogenase endpoint assay. Thus, phosphate buffer should be avoided.

1.5 Synthesis of [$^{15}\text{N-CA}$]-NADH

5 ml of purified [$^{15}\text{N-CA}$]- NAD^+ was used for the enzymatic synthesis of NADH. 5ml of 0.02 units/ml yeast alcohol dehydrogenase (ADH), 5ml of 4.3 mM ethanol, and 10 ml of 50 mM Tris buffer (pH 8.0) were used to synthesis of NADH (Figure 1.5.1). The reaction was run at room temperature until UV-absorbance at 340nm reached a plateau (figure 1.5.2).The concentration of NADH was calculated to be 787 μM , based on absorbance at 340 nm. After the reaction was done, ADH enzyme was removed by ultrafiltration (Millipore, cutoff of 3kDa). The concentration of NADH was determined once more with 5 μL of NADH added to 995 μL of 50 mM Tris buffer at pH 8.0, after blanking with 1ml of 50 mM Tris buffer. The concentration of NADH was calculated to be 614 μM . The solution was flash frozen in liquid nitrogen.

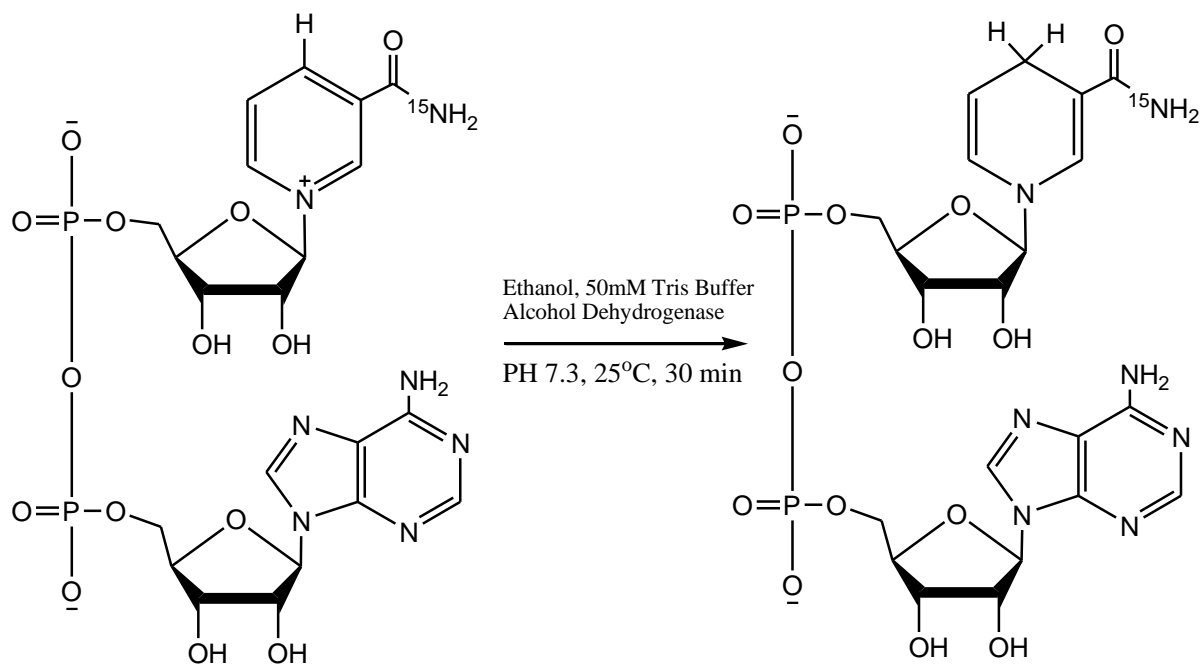


Figure 1.5.1 Synthesis of ^{15}N -NADH

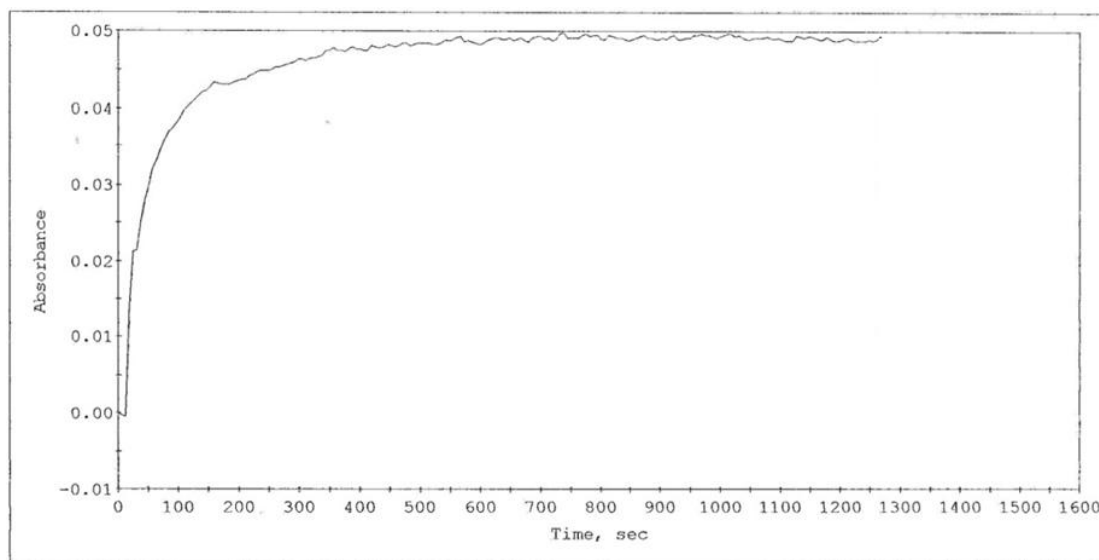


Figure 1.5.2 Alcohol Dehydrogenase enzymatic assay: 10 μL of NAD^+ , 5 μL of 4.3 mM Methanol, 10 μL of 3.73×10^{-5} units/ml of Alcohol dehydrogenase, 975 μL of 50 mM Tris buffer. Absorbance=0.0490, Concentration=787 μM

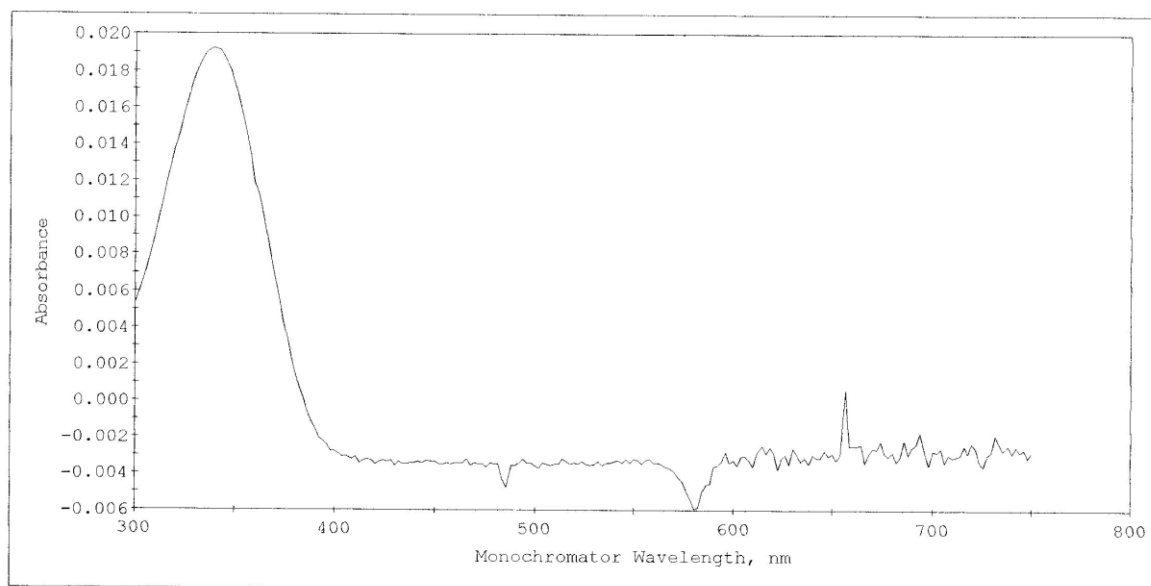


Figure 1.5.3 UV-Vis spectrum (scanned from 300 nm to 800 nm) for 5 μ L of NADH in 995 μ L of 50 mM Tris buffer pH 8.0, Absorbance=0.0191, concentration=614 μ M.

1.6 Synthesis of [¹⁵N-CA]-NADP⁺

5 ml of 5 mM of NADP⁺ (purchased from Sigma), 5 mL of 50 mM of [¹⁵N-CA]-nicotinamide, and 5 mL of 200 units NADase (purchased from Sigma) were added to 10 mL of Tris buffer at pH 7.3. Before starting incubation of the NADase reaction at 37 °C, 1 mL of NADP⁺ and a mixture of 500 uL of NADP⁺ and 500 uL of NADase were prepared as a control sample to confirm the full exchange of [¹⁵N-CA]-nicotinamide with NADP⁺. Control sample and the reaction mixture were started, incubating at 37 °C until UV absorbance of the control sample at 340 nm decreased (50 hours) from 0.0483 to 0.0082 by the cyanide method⁹, as described above. 10 uL of sample was added to 990 uL of 1.0 M NaCN in a 1 ml quartz cuvette, with cyanide solution was used as a blank. The absorbance at 340 nm was appears at 0.0558.

The reaction sample was then heated up to 70 °C for 2 minutes to deactivate the NADase. The deactivated protein was separated by centrifuging at 4000 rpm and supernatant was collected for further purification.

[¹⁵N-CA]-NADP⁺ was further purified using a BioGel P2 gel (Bio-Rad) column with 50mM Tris buffer at pH 7.3. The final concentration of [¹⁵N-CA]-NADP⁺ was determined using 400 uL of DMSO, 40uL of 37.5 mM Glucose, 20 uL of [¹⁵N-CA]-NADP⁺, 2.3 uL Glucose 6 phosphate dehydrogenase (100 units of G6PDH) and 538uL of Tris buffer at PH 7.3, in an enzyme endpoint assay¹⁰. Note the in the presence of DMSO, G6PDH will accept glucose as a substrate, in place of glucose-6-phosphate. Absorbance at 340 nm was 0.390, corresponding to a concentration of [¹⁵N-CA]-NADP⁺ of 3,135 uM. UV-absorbance between 300 and 900 nm was scanned for confirmation of [¹⁵N-CA]-NADPH production; absorbance at 340 nm allowed calculation of a concentration of 3199 uM, consistent with that measured from the first assay. The [¹⁵N-CA]-NADP⁺ stock solution was frozen in liquid nitrogen or lyophilized overnight.

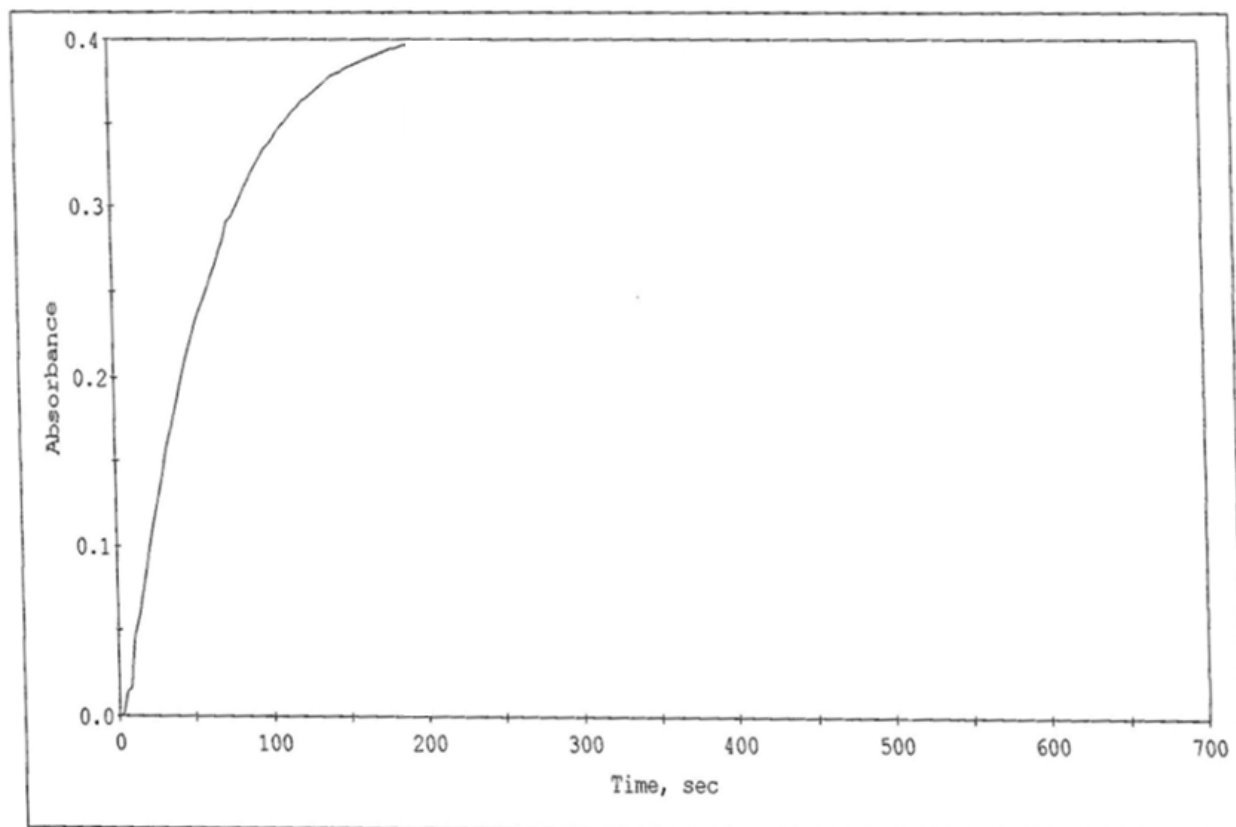


Figure 1.6.1 Enzyme endpoint assay with glucose-6-phosphate dehydrogenase (G6PDH):400 uL of DMSO, 40 uL of 37.5 mM Glucose, 20 uL of [¹⁵N-CA]-NADP⁺, 2.3 uL G6PDH (100 units), and 538uL of Tris buffer at PH 7.3. Concentration=3,135uM.

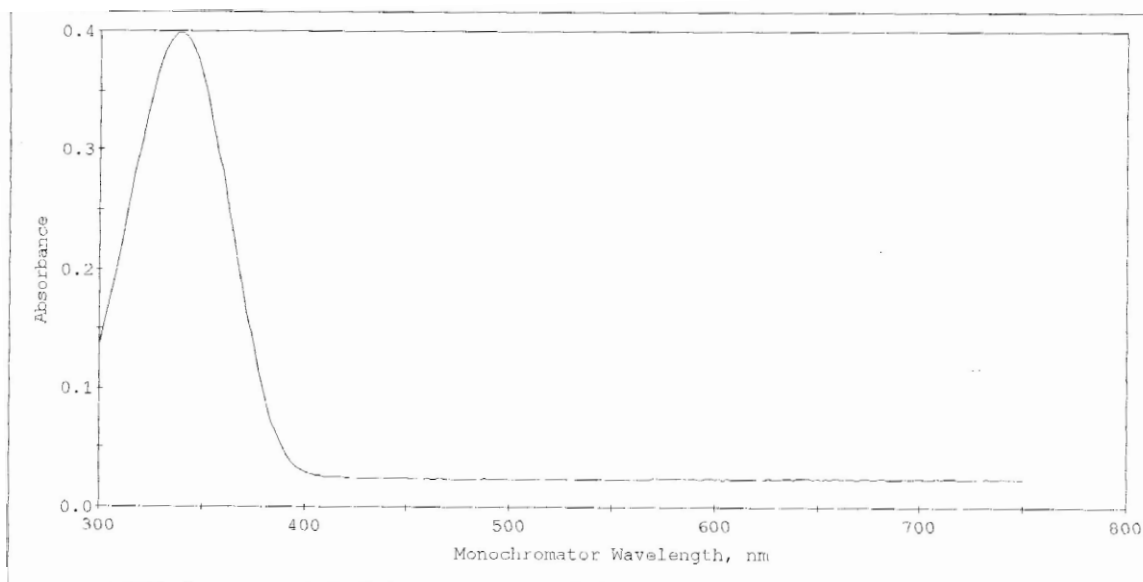


Figure 1.6.2 UV-Vis spectrum (scanned from 300 nm to 800 nm): Expected band is present at 340 nm for NADPH, and confirmation of concentration: 558 uL of 50 mM Tris Buffer, 400 uL of 99.8% DMSO, 40 uL 1.5 M glucose, 2 uL of G6PDH, 20 uL of NADP⁺. Spectrum was taken right after reaction was done. Concentration=3199 uM

1.7 Synthesis of [¹⁵N-CA]-NADPH

5ml of [¹⁵N-CA]-NADP⁺ purified previously was used for enzymatic NADPH synthesis. 0.25ml of a solution that is 100 units/ mL Glucose 6 Phosphate Dehydrogenase, 4 ml of 99.8% DMSO, 0.75 ml of 100 mM Glucose, and 5 ml of [¹⁵N-CA]-NADP⁺ in Tris buffer at PH 8.0 were used for NADPH synthesis. The reaction was run at room temperature until UV-absorbance at 340 nm reached a plateau, at 0.230 (Figure 1.7.1). The calculated concentration of [¹⁵N-CA]-NADPH based on absorbance at 340 nm was 1848 uM. After the reaction was done, Glucose-6-Phosphate Dehydrogenase enzyme was removed by ultrafiltration (Millipore, cutoff of 3kDa). The solution of [¹⁵N-CA]-NADPH was lyophilized to remove solvent.

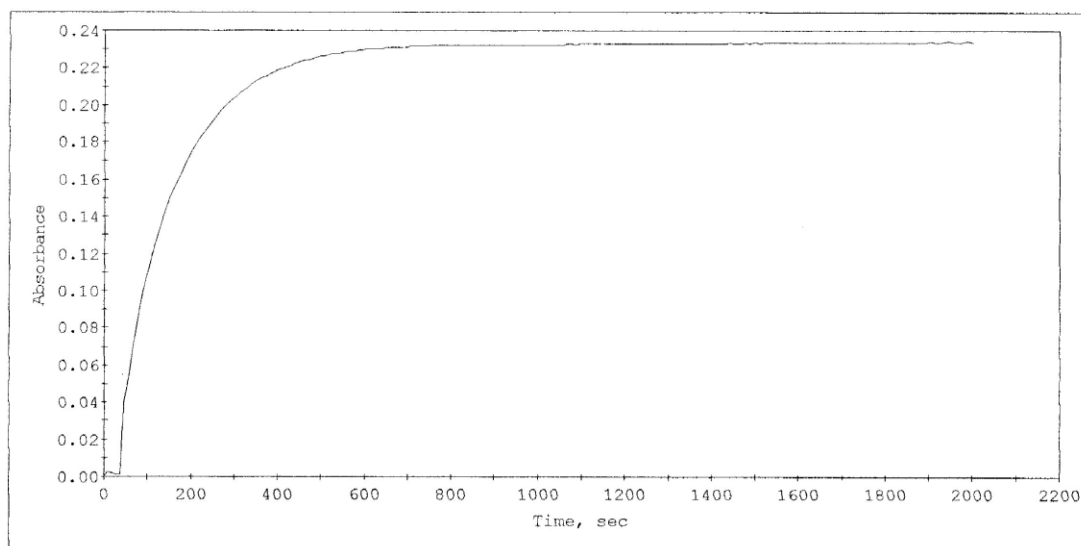


Figure 1.7 Glucose-6-phosphate Dehydrogenase (G6PDH) endpoint assay: 125 μL of 100 units Glucose 6 Phosphate Dehydrogenase, 400 μL of 99.8% DMSO, 75 μL of 100mM Glucose, and 20 μL [^{15}N -CA]-NADP $^{+}$ in 480 μL Tris buffer at pH 8.0. Absorbance=0.230, concentration=1848 μM .

1.8 1D HSQC

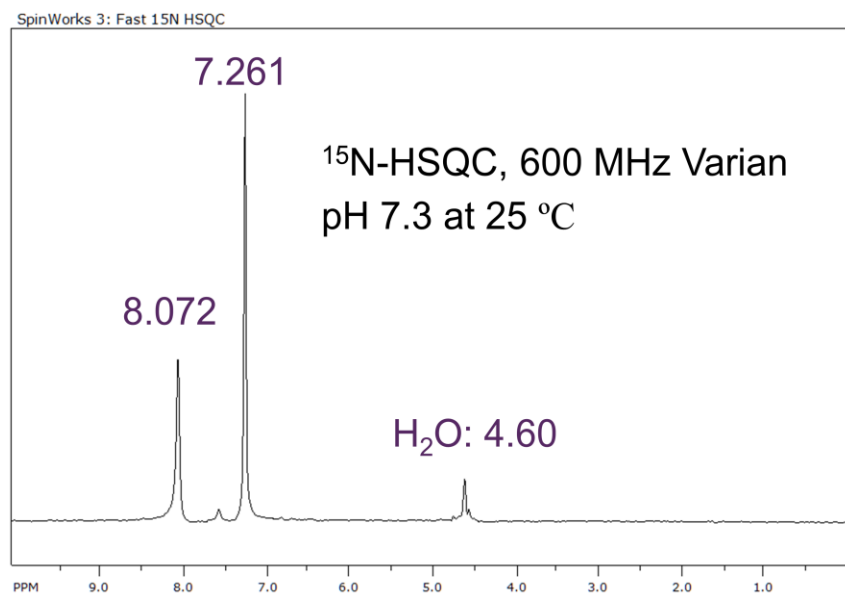


Figure 1.8.1 1D- ^{15}N -filtered HSQC of ^{15}N -NAD $^{+}$

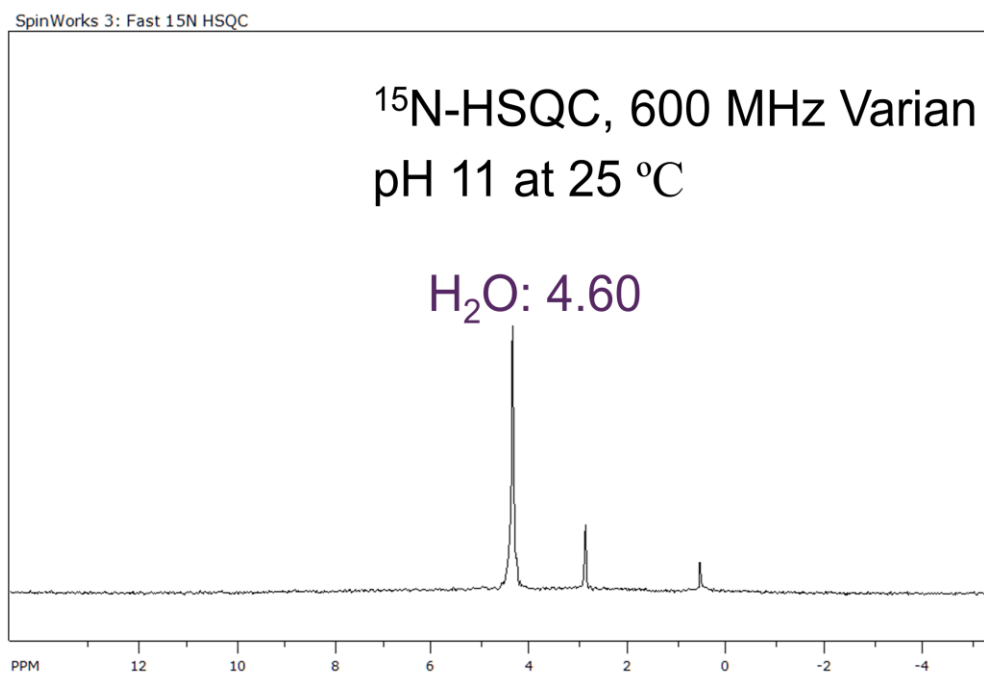


Figure 1.8.2 1D- ^{15}N -filtered HSQC of ^{15}N -NADH at pH 11

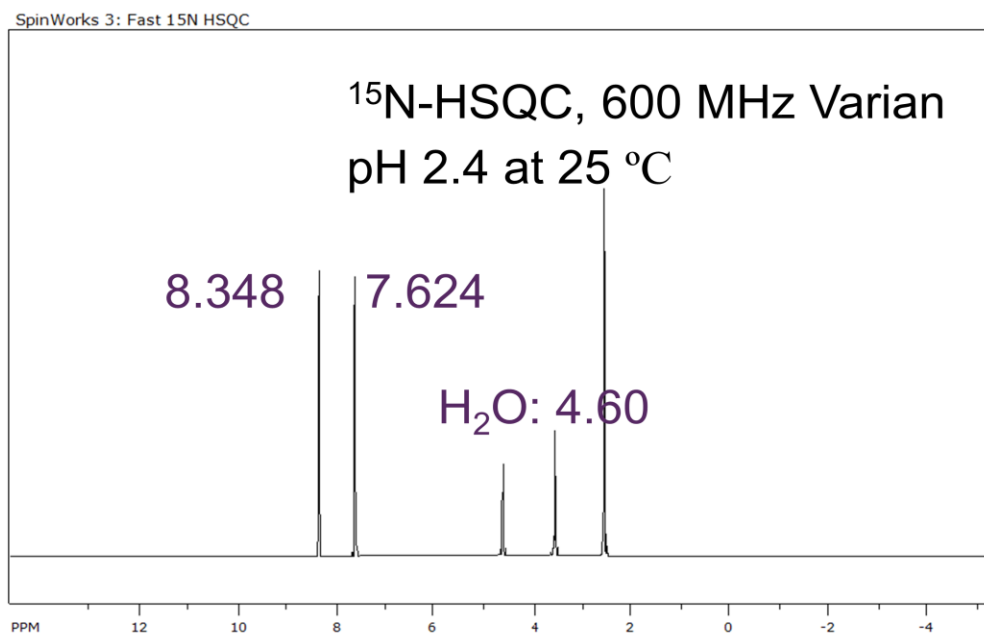


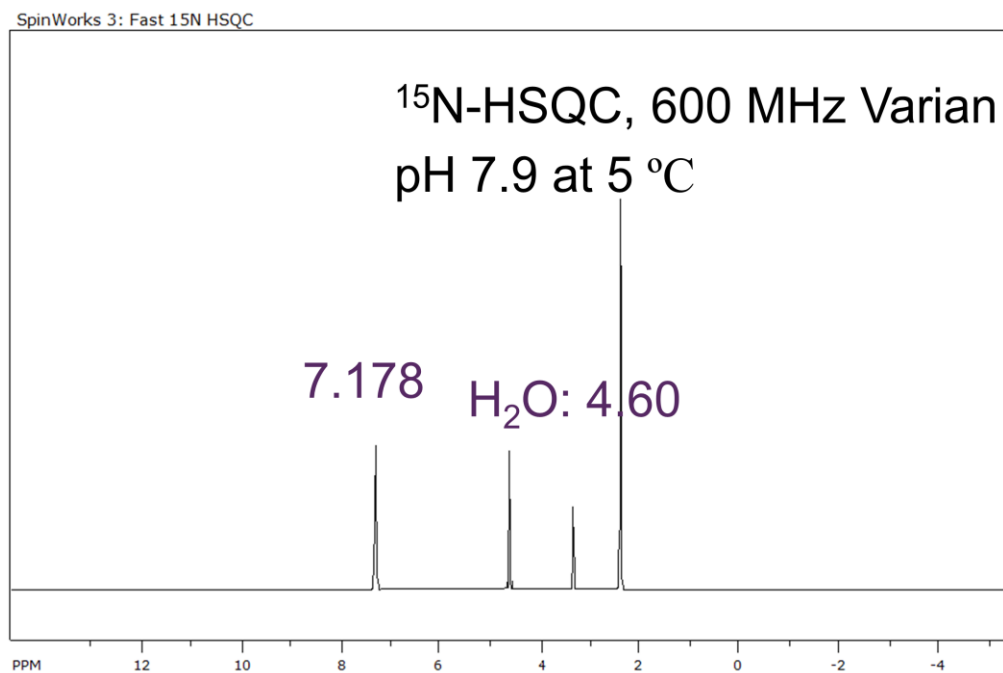
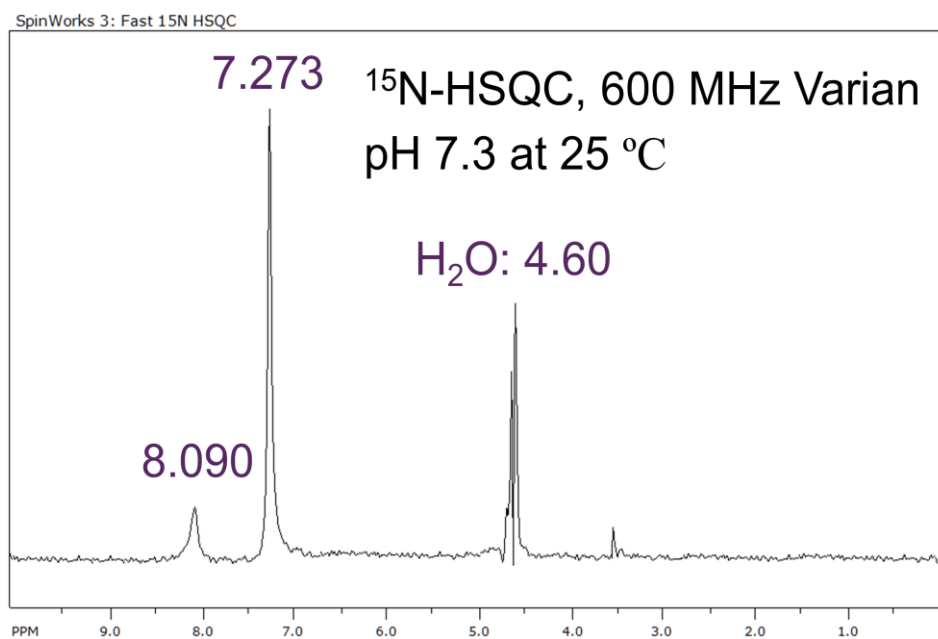
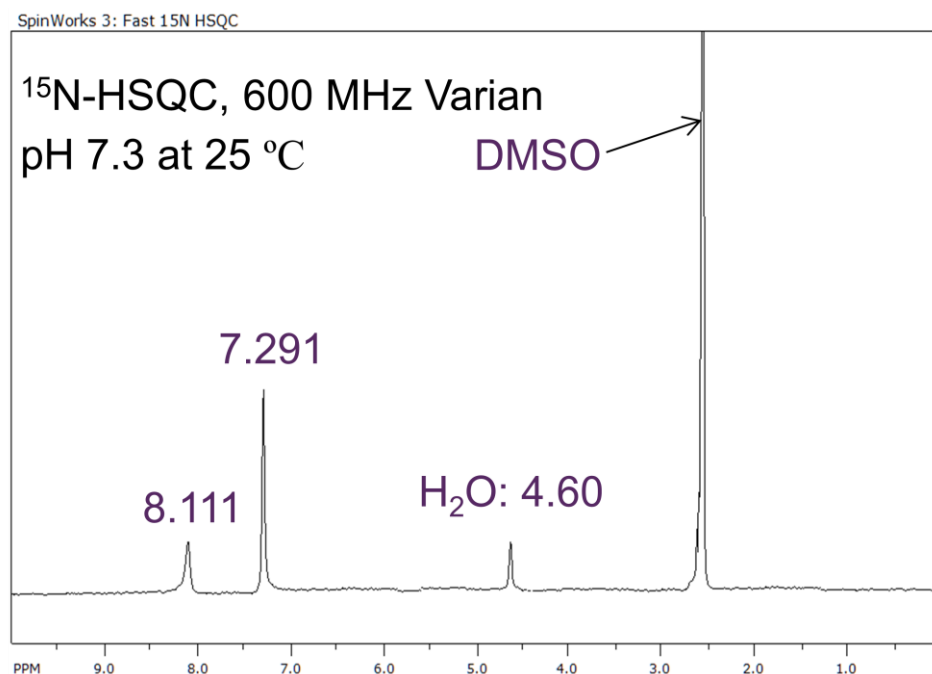
Figure 1.8.3 1D-¹⁵N-filtered HSQC of ¹⁵N-NADH at pH 2.4**Figure 1.8.4 1D-¹⁵N-filtered HSQC of ¹⁵N-NADH at Temperature 5°C**

Figure 1.8.5 1D-¹⁵N- filtered HSQC of NADP⁺**Figure 1.8.6 1D-¹⁵N- filtered HSQC of NADPH**

1D-HSQC was collected on a 600 MHz Varian spectrometer at room temperature. The water peak was used as a reference and calibrated at 4.6 ppm.

The chemical shift of H-anti between NAD⁺ and NADP⁺ was from 8.072 to 8.090. The chemical shift of H-syn between NAD⁺ and NADP⁺ was from 7.261 to 7.273.

The chemical shift of H-anti between NADP⁺ and NADPH was from 8.090 to 8.111. The chemical shift of H-syn between NAD⁺ and NADP⁺ was from 7.273 to 7.291.

After synthesis of NADH, pH of NADH in Tri buffer solution was adjusted to 11 due to stability of cofactor at different pH (Section 1.4.) At the high pH (pH: 11), No peaks from hydrogens on carboxamide

were observed at room temperature (Figure 1.8.2). No peaks from hydrogens on carboxamide were observed at pH 7.9 and room temperature. At the reduced temperature (5 °C), only one peak from hydrogens on carboxamide was observed at pH 7.9. pH was reduced to 2.5 and two peaks from hydrogens on carboxamide were observed.

From 1D-HSQC, the synthesis of ^{15}N -labeled cofactors were confirmed.

1.9 Results and Discussion

$[^{15}\text{N}\text{-CA}]\text{-NAD(H)}$ was synthesized successfully and the concentration and activity of the cofactor were confirmed with alcohol dehydrogenase assays by UV-vis spectroscopy. The concentration of $[^{15}\text{N}\text{-CA}]\text{-NAD}^+$ was not changed after several freeze-thaw cycles in a pH range between 2 and 7.3 in Tris buffer. $[^{15}\text{N}\text{-CA}]\text{-NADH}$ was stable in the pH range between 7.3 and 12 in Tris buffer. NAD^+ is known to be base labile, and NADH is acid labile, so careful attention to pH is important when storing cofactor for extended periods

$[^{15}\text{N}\text{-CA}]\text{-NADP(H)}$ was synthesized successfully and the concentration and activity of the cofactor was confirmed with a G6PDH endpoint assay in 40% DMSO. The concentration of $[^{15}\text{N}\text{-CA}]\text{-NADP}^+$ was not changed after several freeze-thaw cycles in the pH range between 2 and 7.3 in Tris buffer. $[^{15}\text{N}\text{-CA}]\text{-NADPH}$ was stable in the pH range between 7.3 and 12 in Tris buffer.

1.10 Conclusion

^{15}N -labeled cofactors NAD(P)(H) have been synthesized successfully. The problem with stability of these cofactors was resolved by using Tris buffer instead of phosphate buffer. After 8 freeze-thaw cycles over one month, the concentration was maintained, as assessed by UV-Vis spectroscopy analysis. The 1D-HSQC spectra confirmed that ^{15}N -labeled cofactors NAD(P)(H) were produced. These ^{15}N labeled cofactors will be used as probes to study cofactor geometry with ^{15}N NOESY, and in dynamics studies using CPMG-based relaxation dispersion measurements.

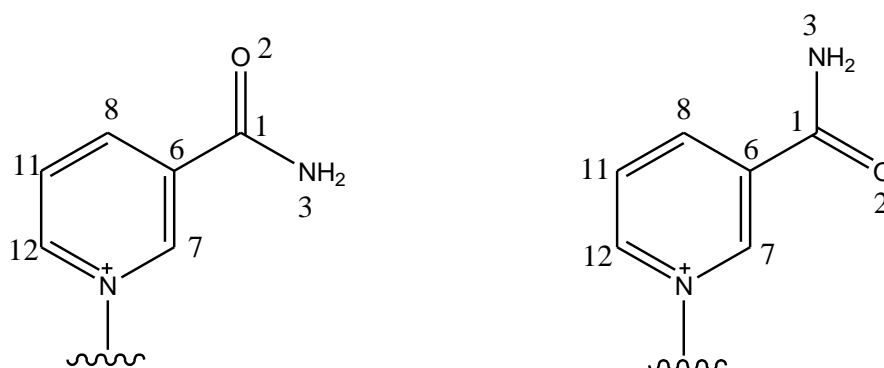
2. Introduction

Enzymatic structure and dynamics have been studied with various computational methods along with NMR and X-ray crystallography studies¹¹. Certain structural questions regarding cofactors in oxidoreductase reactions, regarding the conformation of the NAD(P)(H) (Figure 2.3 and Figure 2.4) cofactor, are of interest in the studies presented herein. Of particular interest is conformation and dynamics of the nicotinamide ring when bound to enzymes, since orientation of the carboxamide group is often ambiguous due to the limitation of X-ray crystallography. In X-ray crystallography analysis, the Nitrogen and Oxygen in the amide group in Nicotinamide Nucleotides is often not easy to distinguish¹⁰⁵. Both dihedral angle $X \approx 180^\circ$ position^{16,17} of amide and dihedral angle $X \approx 0^\circ$ position^{10, 18,19, 20} of amide are possible (figure 2.1), although both are not observed with equal frequency – suggesting one orientation is either more favorable energetically, or more suitable for the reaction catalyzed by oxidoreductases.

Thus, our interest is the dihedral angle, C3- C2- C6- O' (figure 2.2), of the amide in the nicotinamide ring of the NAD(P)(H) cofactor. The dihedral angle, $X \approx 0^\circ$, of C3-C2-C6-O' in nicotinamide adenine dinucleosides (figure 2.2) was observed in X-ray crystallography about 90% of the time according to a survey of crystal structures reported by the Sem lab. The opposite angle, $X \approx 180^\circ$, of C3-C2-C6-O' in the nicotinamide ring was observed only about 10% of the time. ¹⁵N –filtered NOESY measurements with ¹⁵N labeled cofactors will be used confirm this results, or correct errors that may have been made, based on improper determination of Nitrogen and Oxygen atoms of the amide in X-ray crystal structures (perhaps the $X \approx 180^\circ$ conformation

is observed 100% of the time). Computational studies are used to explore and propose the rationale for any preferred conformations and mechanisms, by analysis of energy, charge, and resonance structures of NAD(P)(H) cofactors and simplified model derivatives, using Gaussian 9 and NBO5.

Understanding of structural preferences and mechanism will help to improve our understanding of the hydride transfer reaction involving NAD(P)⁺ and NAD(P)H with oxidoreductase enzymes. This understanding may also facilitate drug design efforts, where inhibitors are rationally designed to bind cofactor binding sites, or that span cofactor and substrate binding sites



Dihedral angle (X) of C8-C6-C1-O2 = 0 degree Dihedral angle (X) of C8-C6-C1-O2 = 180 degree
 Figure 2.1 Dihedral angle (X) of carboxamide X $\approx 0^\circ$ on the left, and dihedral angle (X) of carboxamide X $\approx 180^\circ$ on the right

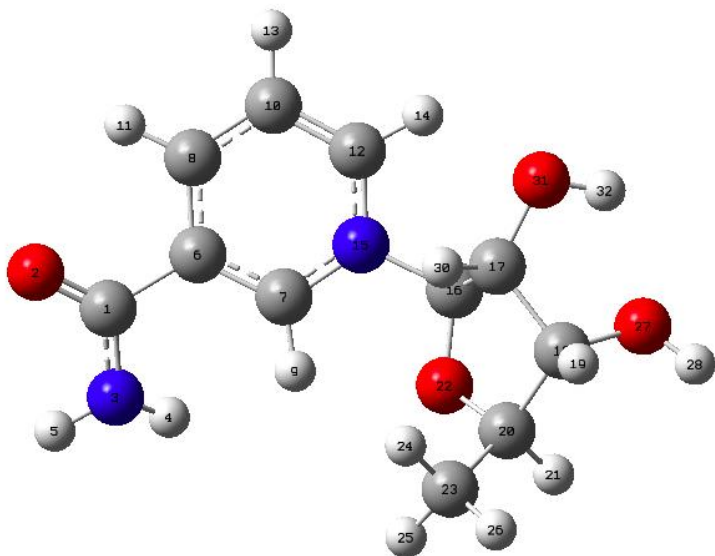


Figure 2.2 Numbered atoms in Nicotinamide nucleoside as used for Gaussian calculation, Dihedral angle of O2-C1-C6-C8 is called X, The figure shows an example of $X \approx 0^\circ$.

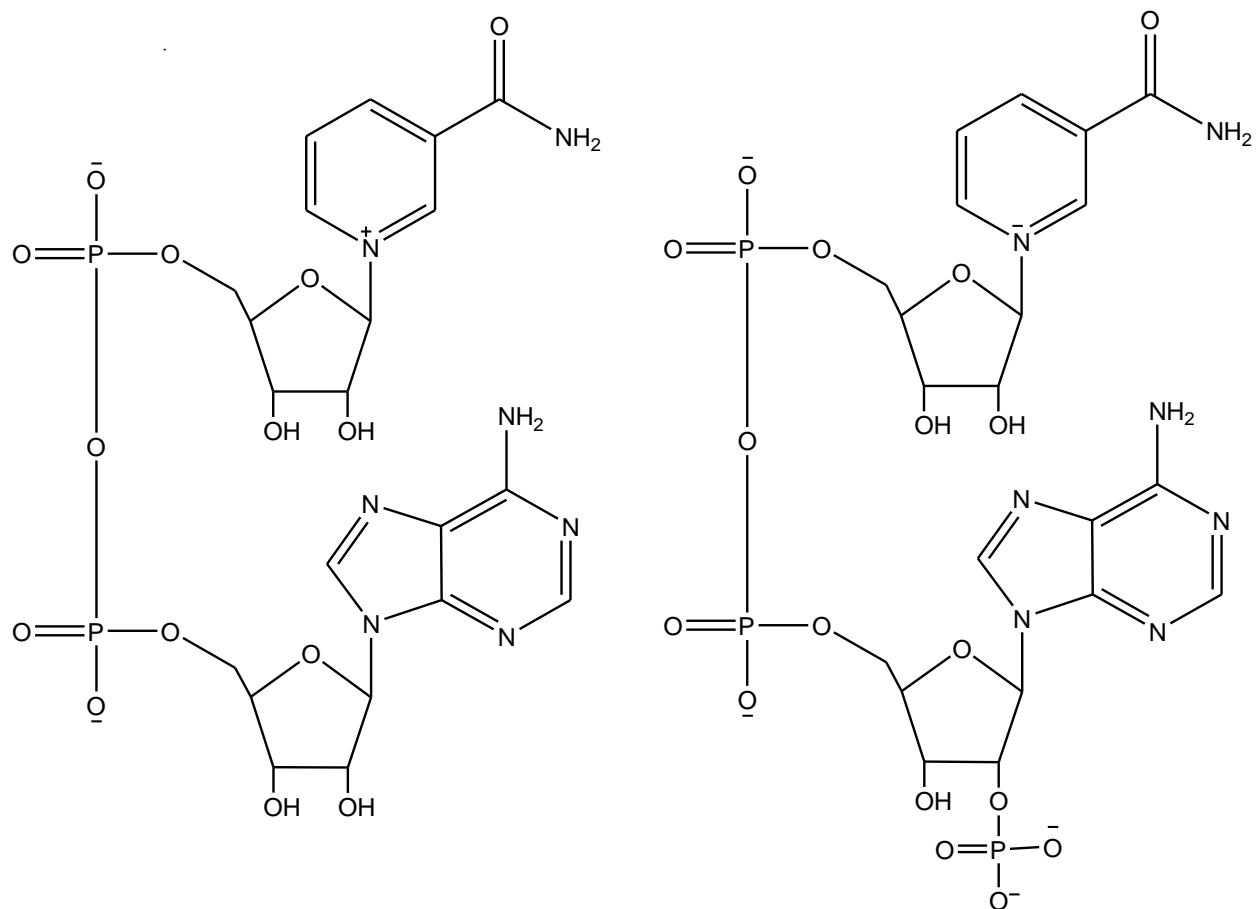


Figure 2.3. Nicotinamide Adenine Dinucleotide, Oxidized Form (NAD⁺) on the left; Nicotinamide Adenine Dinucleotide Phosphate, Oxidized Form (NADP⁺) on the right

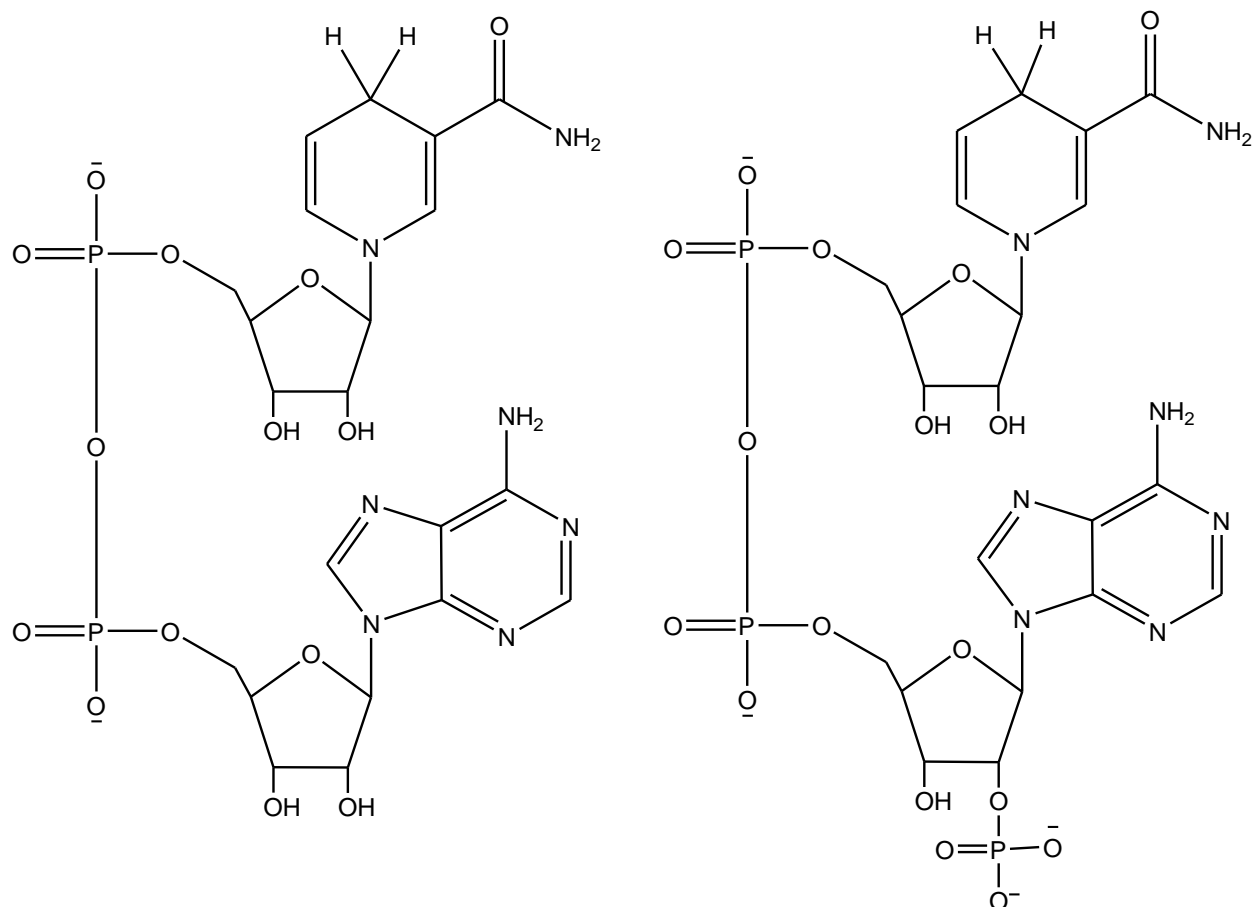


Figure 2.4 Nicotinamide Adenine Dinucleotide, Reduced Form (NADH) on the left; Nicotinamide Adenine Dinucleotide Phosphate, Reduced Form (NADPH) on the right

2.1 Materials and Methods

Herein, we used Gaussian 9.0 and NBO5 on Marquette's Pere cluster. Gaussian 9 is used for geometric optimization and analysis of energy, charge, spectroscopy, and structure with Density map function (DMF). The hybrid density functional b3lyp with 6-31(G) basis sets was used for analysis. After optimization with Gaussian 9, input files from Gaussian 9.0 were used for NBO5, which was provided from Dr. Timerghazin, for resonance structure calculations.

Simplified derivatives (model compounds) of reduced or oxidized forms of Nicotinamide Adenosine Dinucleotide (Phosphate), NAD(P)(H), were drawn in Gaussian View (Figure 2.2). The input file was edited as in Figure 2.1.1, and Gaussian geometric optimizations performed, using b3lyp/6-31g(d).

```
%chk=/home/MARQNET/9000kimj/NAD/N-down_nicotinide.chk
# opt freq b3lyp/6-31g(d)

N-down_nicotinide.com

1 1
C          -3.02843746      0.92289510     -0.35270263
O          -4.09873570      1.42246532      0.08141927
N          -2.36261464      1.51427073     -1.52225589
H          -1.37580066      1.36772884     -1.45352711
H          -2.70657689      1.08179355     -2.35571462
C          -2.41616077     -0.30800368      0.34127536
r          -1.77475770     -0.86048104     -0.17605767
```

Figure 2.1.1 Geometry optimization input file

The output file from geometric optimization was edited for geometric check or rotational energy calculation or spectroscopy analysis (Figure 2.2.2). The output file from geometric check was also edited to create the NBO input file (Figure 2.2.3). Additionally, bond length, charge, dihedral angle, vibration, and energy scan results were analyzed with Gaussian View.

```

%chk=/home/MARQNET/9000kimj/NAD/N-down_nicotinide.chk
#p b3lyp/6-31g* Opt=ModRed pop=nboread
geom=check guess=read

N-down_nicotinide.com

1 1

2 1 6 7 S 36 10.0 0.0 360.0

$nb0 archive file=myjob $end

~
-

```

Figure 2.1.2 Input file for geometric check or rotational energy calculation or spectroscopy calculations.

```

$GENNBO NATOMS=32 NBAS=285 UPPER BODM $END
$NBO NRT $END
$COORD
N-down_nicotinide.com
  6   6   -3.847324   -0.649350   0.119409
  8   8   -4.757795   -0.321316   0.859623
  7   7   -3.808849   -1.815380  -0.585835
  1   1   -3.239679   -1.920599  -1.414338
  1   1   -4.646501   -2.384596  -0.544843
  6   6   -2.635347    0.256460   0.002579
  6   6   -1.371769   -0.194076  -0.343633
  6   6   -2.793023    1.606157   0.354249
  1   1   -1.138650   -1.228574  -0.575868
  6   6   -1.698582    2.464305   0.312780
  1   1   -3.776687    1.947367   0.661148
  6   6   -0.454829    1.964300  -0.049146
  1   1   -1.793716    3.514686   0.564031
  1   1    0.449473    2.556040  -0.106035

```

Figure 2.1.3 Input file for NBO5 calculations.

2.2. Rotational Energy of NAD(P)(H)

Recent article published for x-ray crystallography related to NAD(P)(H) shows the conformation of amide position, $X \approx 0^\circ$, is the most abundant. Analysis of potential energy according to the rotation of amide in NAD(P)(H) provides understanding of relationship between the most abundant and the most stable structure. If the most abundant structure is not the most stable structure, enzymatic catalyst reaction has to at least overcome this energy cap additionally. This may be a clue for rationalization of enzymatic reaction in the aspect of cofactors.

The potential energies were calculated as a function of the bond rotation between C1 and C6, amide structure in Nicotinamide. The bond was rotated every 10° from 0° to 360° . The structure of the cofactor, NAD(P)(H), is a relatively large molecule for a computational study. Because the effects from distal elements are likely to be insignificant, simplified derivative molecules, Propene, Nicotinamide, and Nicotinamide nucleoside of NAD(P)(H) were used for geometry optimization and other computational studies.

STUDIES OF OXIDIZED NICOTINAMIDE RING AND ANALOGS

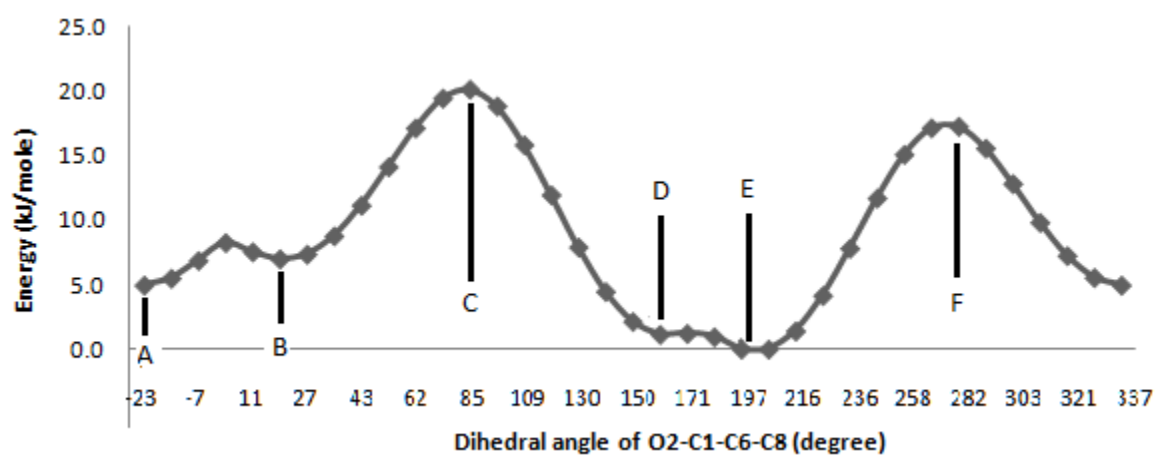


Figure 2.2.1 **Rotational Energy of C1-C6 bond in Oxidized NicotinamideNucleoside**, $X=0^\circ$ is Dihedral angle of O2-C1-C6-C8 = 0° , Structure "A" was geometrically optimized.

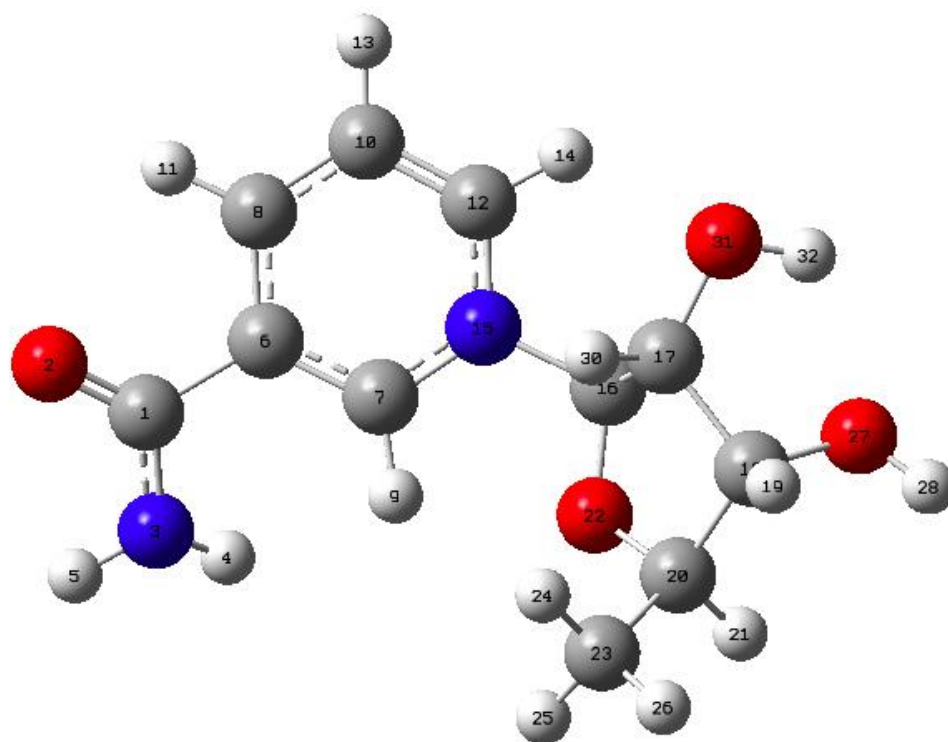


Figure 2.2.2 Structure A from energy diagram in Figure 2.2.1, at $X = -22.66^\circ$, Energy = 5.0 KJ/mole. The glycosidic bond (N15-C16) is in the syn conformation.

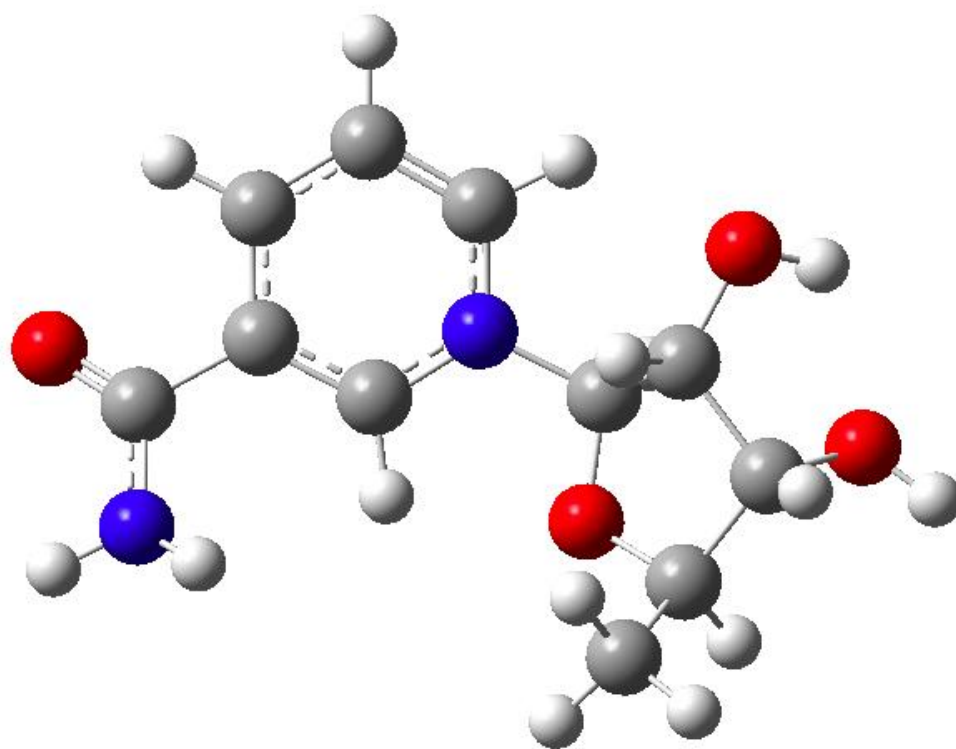


Figure 2.2.3 Structure B from energy diagram in Figure 2.2.1, $X = 19.01^\circ$, Energy = 7.0 KJ/mole.

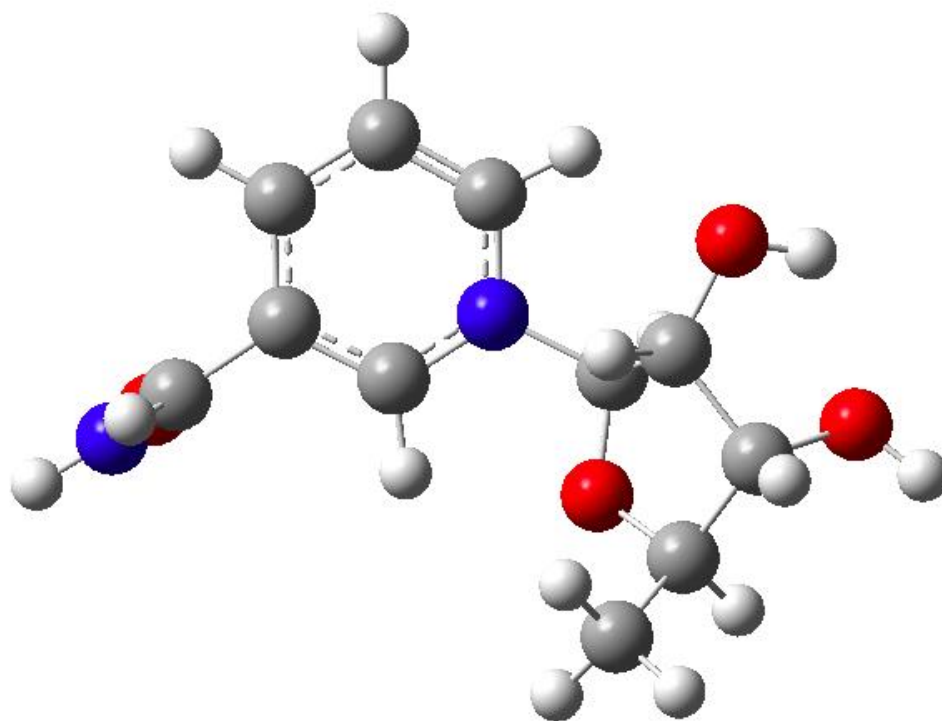


Figure 2.2.3 Structure C from energy diagram in Figure 2.2.1, $X = 85.42^\circ$, Energy = 20.1 KJ/mole.

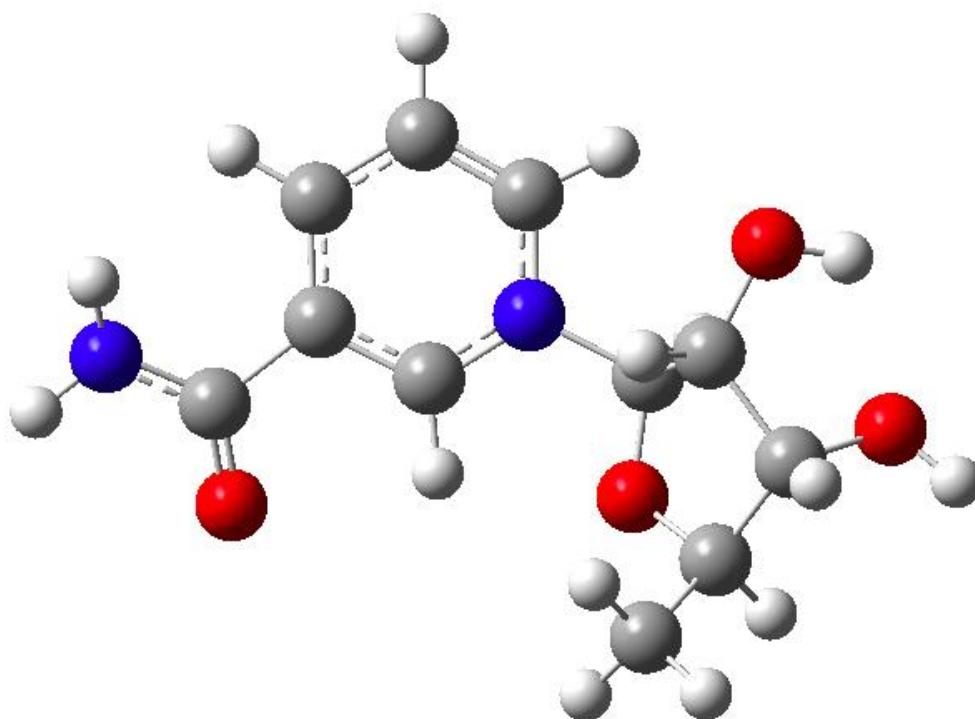


Figure 2.2.4 Structure D from energy diagram in Figure 2.2.1, $X = 160.17^\circ$, Energy = 1.2 KJ/mole.

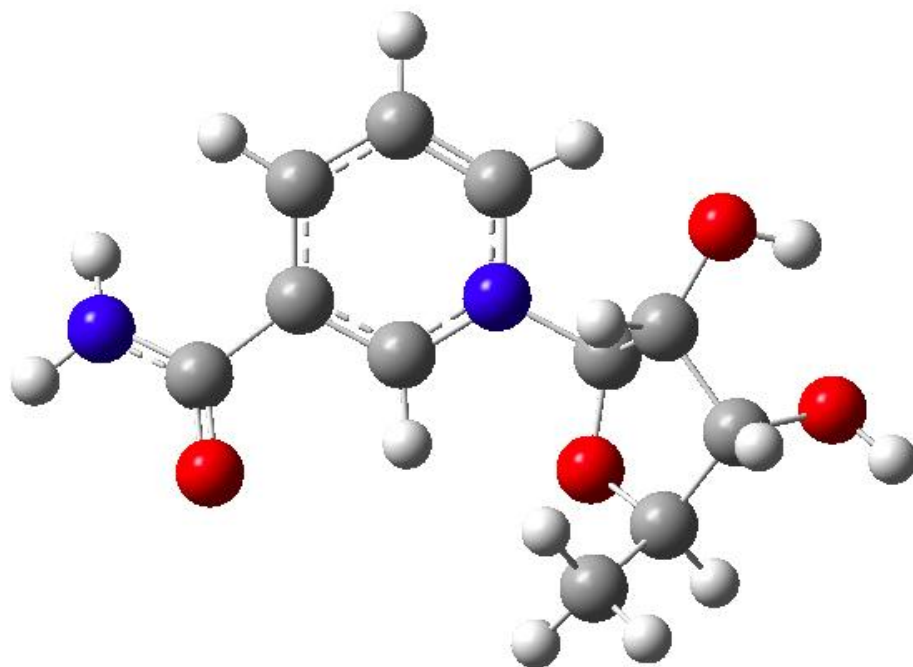


Figure 2.2.5 Structure E from energy diagram in Figure 2.2.1, $X = 206.60^\circ$, Energy = 0.0 KJ/mole.

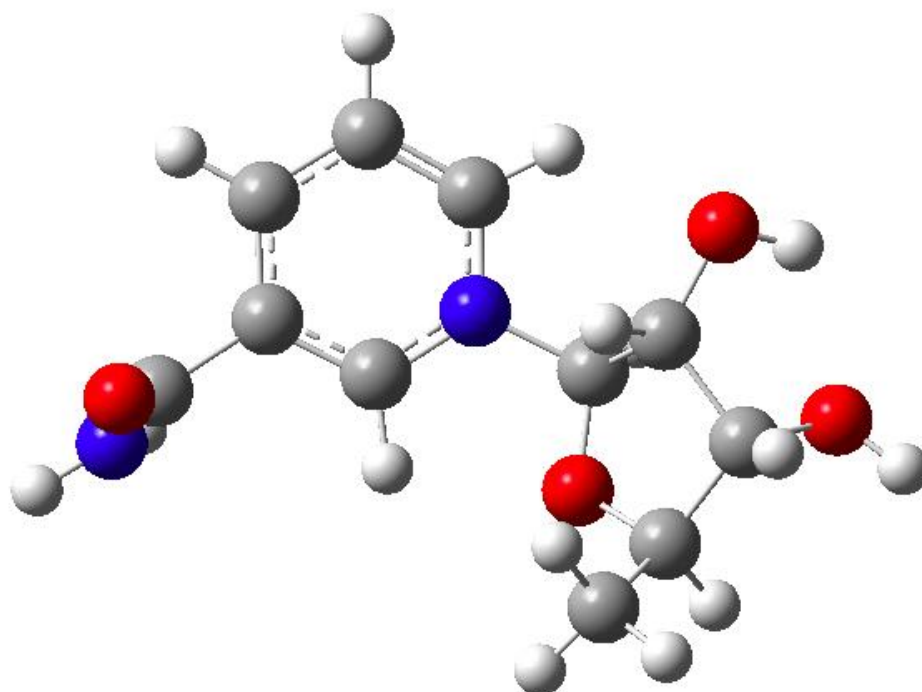


Figure 2.2.6 Structure F from energy diagram in Figure 2.2.1, $X = 281.60^\circ$, Energy = 17.3 KJ/mole.

Preferred geometry for the carboxamide group. The dihedral angle of O2-C1-C6-C8 = 0° was set as $X = 0^\circ$. The energy of rotational energy was normalized to the lowest energy structure, Structure “E”, which had $X \approx 180^\circ$, potential energy = 0 KJ/mole. The potential energy of $X = -22.7^\circ$, $X = 0^\circ$, and $X = 19.0^\circ$ structures were 5.0 KJ/mole, 7.9 KJ/mole, and 7.0 KJ/mole respectively. Comparing all conformations, the $X = -22.7^\circ$ structure is the stable and in local minimum as a structure “A”. This conformation is called the $X \approx 0^\circ$ structure.

The potential energy of $X=160.2^\circ$, $X=180.0^\circ$, and $X=206.6^\circ$ structures were 1.2 KJ/mole, 1.1 KJ/mole, and 0.0 KJ/mole respectively. Among these three structures, the $X=206.6^\circ$ structure is the most stable (structure "E"). This conformation is called the $X \approx 180^\circ$ structure. Therefore, the most stable structure of Nicotinamide is Structure "E" over all. The energy difference between structures "A" and "E" is 5.0 KJ/mole. Therefore, an enzyme would need to overcome at least 5.0 KJ/mole to bind the less favored $X \approx 0^\circ$ geometry more favorably. This may, therefore, explain why the $X \approx 0^\circ$ geometry is the one that is observed more commonly in crystal structures.

The carboxamide is not planar. There is steric hindrance between the Hydrogen attached to the carboxamide nitrogen (N3) in the amide group and the hydrogen attached to carbon C7 (also to C8, in the other conformation). The actual distance between hydrogens is below 2.50 Å. Therefore, the $X = 0^\circ$ structure is not as stable a conformation compared to the other two structures ($X = -22.7^\circ$ and $X = 19.0^\circ$) that show a 20 degree distortion from planarity, to overcome the steric hindrance. But, the small energy differences suggest that even modest interactions with enzymatic groups could allow a range of geometries between -20 and +20 degrees.

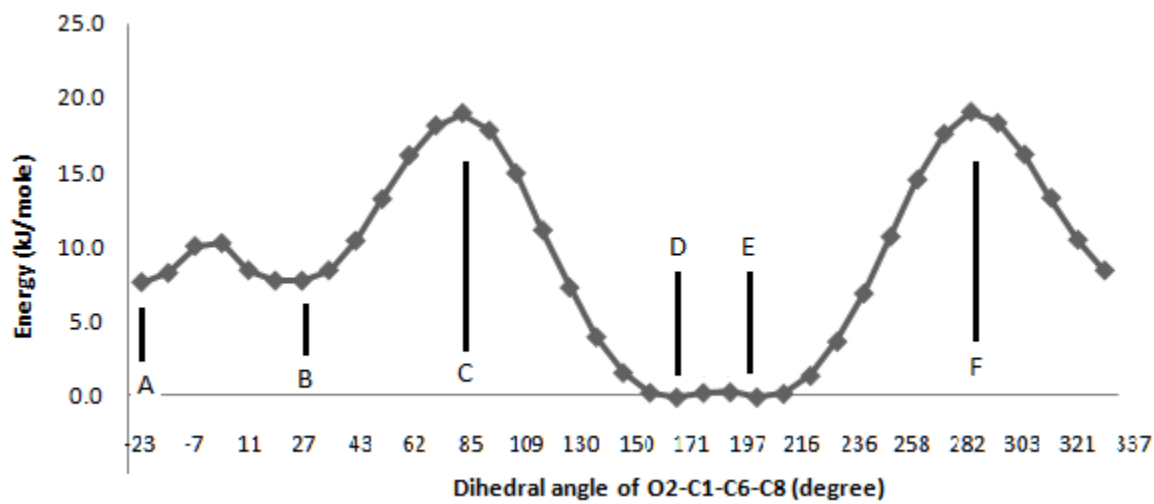


Figure 2.2.7 **Rotational Energy of C1-C6 bond in Oxidized Nicotinamide**, X= 0 ° is Dihedral angle of O2-C1-C6-C8 =0 °, Structure “A” was geometrically optimized. This energy profile, in comparison with that in Fig. 2.2.1, is for the nicotinamide ring with a methyl attached to the pyridine nitrogen, rather than the full ribose ring.

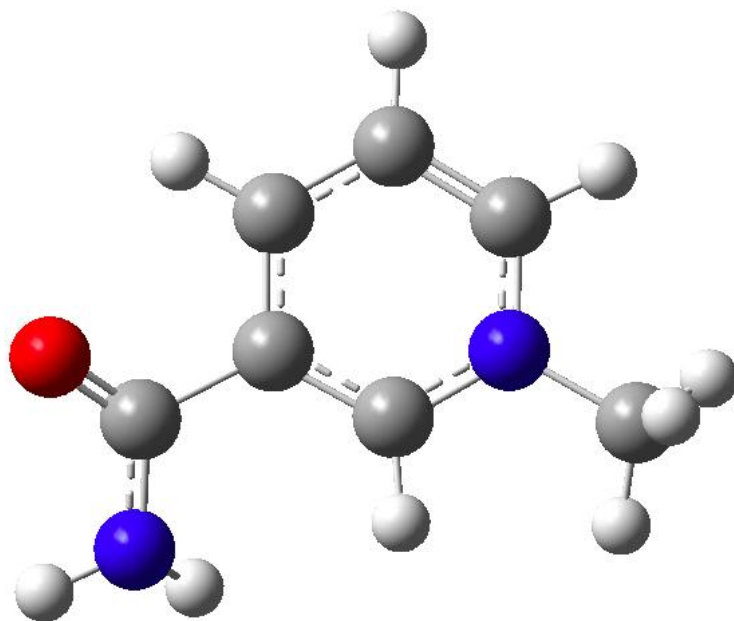


Figure 2.2.8 Structure A from energy diagram in Figure 2.2.7, $X = -25.56^\circ$, Energy = 7.7 KJ/mole.

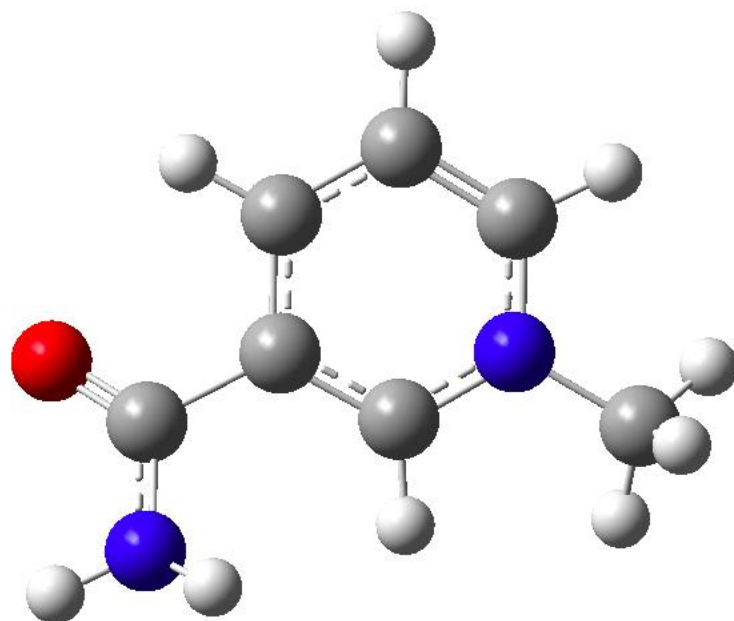


Figure 2.2.9 Structure B from energy diagram in Figure 2.2.7, $X = 24.44^\circ$, Energy = 7.8 KJ/mole.

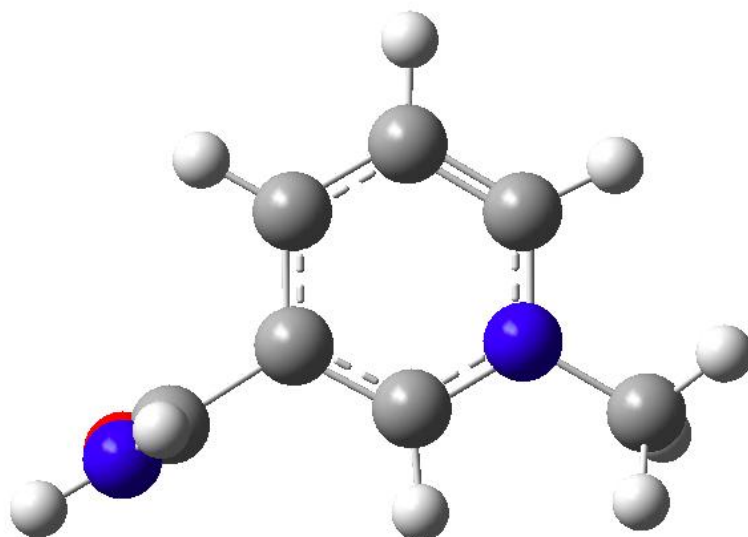


Figure 2.2.10 Structure C from energy diagram in Figure 2.2.7, $X = 84.45^\circ$, Energy = 19.0 KJ/mole.

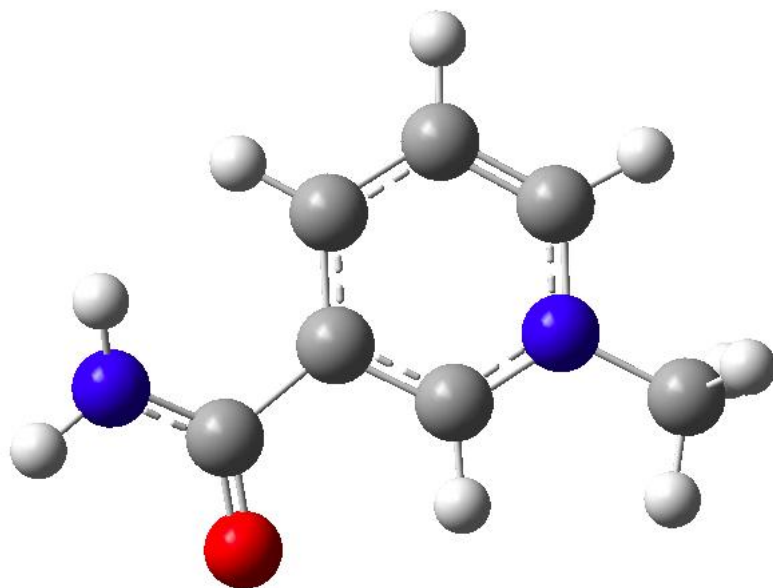


Figure 2.2.11 Structure D from energy diagram in Figure 2.2.7, $X = 154.45^\circ$, Energy = 0.3 KJ/mole.

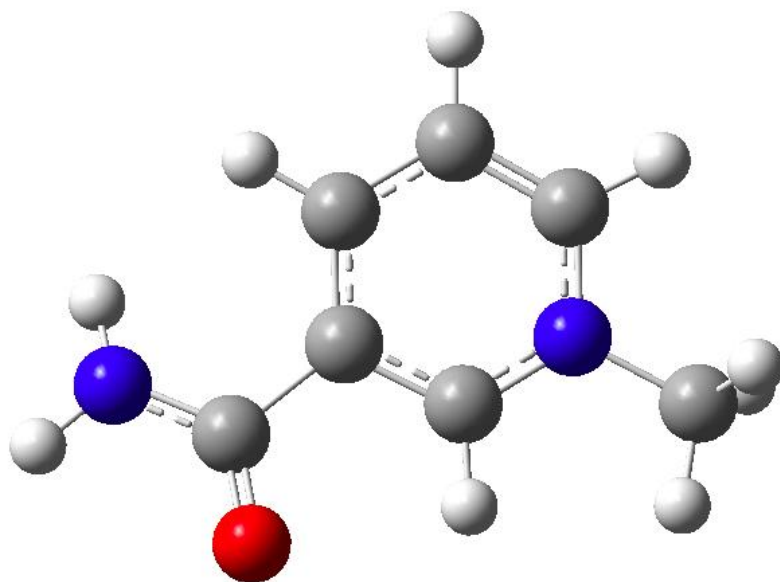


Figure 2.2.12 Structure E from energy diagram in Figure 2.2.7, $X = 194.45^\circ$, Energy = 0.0 KJ/mole

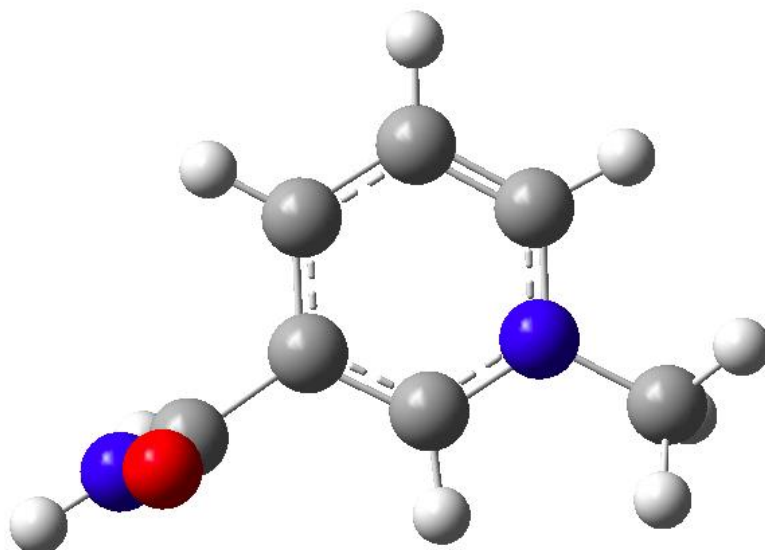


Figure 2.2.13 Structure F from energy diagram in Figure 2.2.7, $X = 264.45^\circ$, Energy = 17.6 KJ/mole.

The dihedral angle of $O2-C1-C6-C8 = 0^\circ$ was set as $X = 0^\circ$, and the energies were normalized to the lowest energy structure, Structure “E”, which had $X \approx 180^\circ$, potential energy = 0 KJ/mole. The potential energy of $X = -25.56^\circ$, $X = 0^\circ$, and $X = 24.44^\circ$ structures were 7.7 KJ/mole, 8.1 KJ/mole, and 7.8 KJ/mole respectively. Among the three structures, the $X = -25.56^\circ$ structure (structure “A”) is a local minimum. This conformation is called the $X \approx 0^\circ$ structure.

The potential energies of the $X = 154.45^\circ$, $X = 180.0^\circ$, and $X = 194.45^\circ$ structures are 0.3 KJ/mole, 0.3 KJ/mole, and 0.0 KJ/mole respectively. Among three structures, the $X = 194.45^\circ$

structure (structure “E”) is the most stable and in a global minimum. This conformation is referred to as the $X \approx 180^\circ$ structure. Therefore, the most stable structure of Oxidized Nicotinamide is Structure “E”, the same as when the full ribose ring was present (see Fig. 2.2.1). The energy difference between structure “A” and “E” is 7.7 KJ/mole. This is a somewhat larger difference (by 2.7 KJ/mol) than was observed in the presence of the ribose ring, but still reflects the same geometric preference for the carboxamide group, which is opposite to the preference found most often for cofactor bound to enzyme.

As before, there is steric hinderance between Hydrogen the carboxamide amide nitrogen (N3) in the amide group and the hydrogen attached to carbon C7 (also to C8, in the other conformation). The actual distance between hydrogens is below 2.57 \AA . Therefore, the $X = 0^\circ$ structure is not as stable a conformation compared to the other two structures: $X = -25.56^\circ$ and $X = 24.44^\circ$.

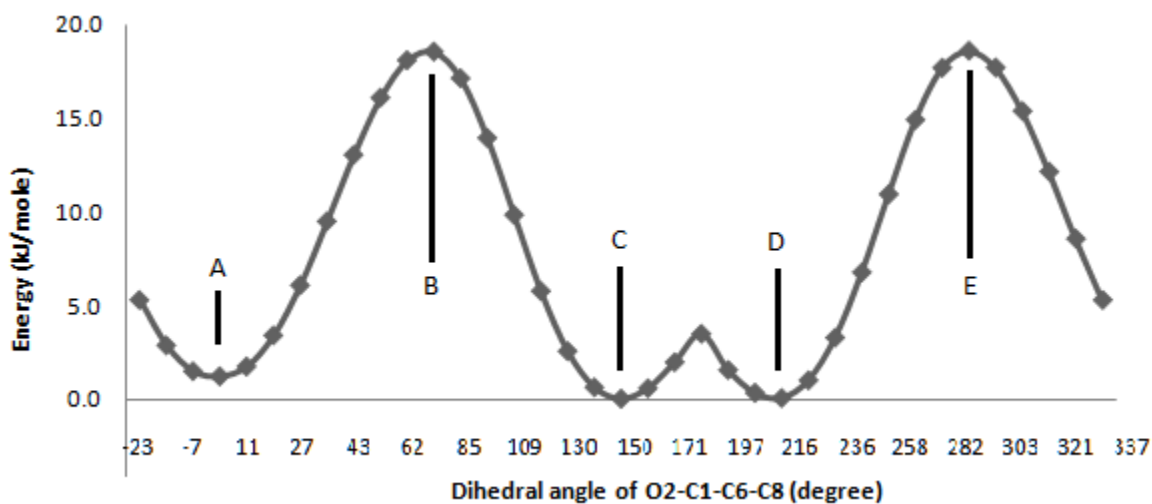


Figure 2.2.14 **Rotational Energy of C1-C6 bond in Propene Carboxamide**; $X = 0^\circ$ is the Dihedral angle of $O2-C1-C6-C8 = 0^\circ$, and Structure "A" was geometry optimized. Compared to energy diagrams in Figures 2.2.1 and 2.2.7, this is a much simpler model compound, with propene in place of the pyridine ring, which is attached to the carboxamide group that is being rotated.

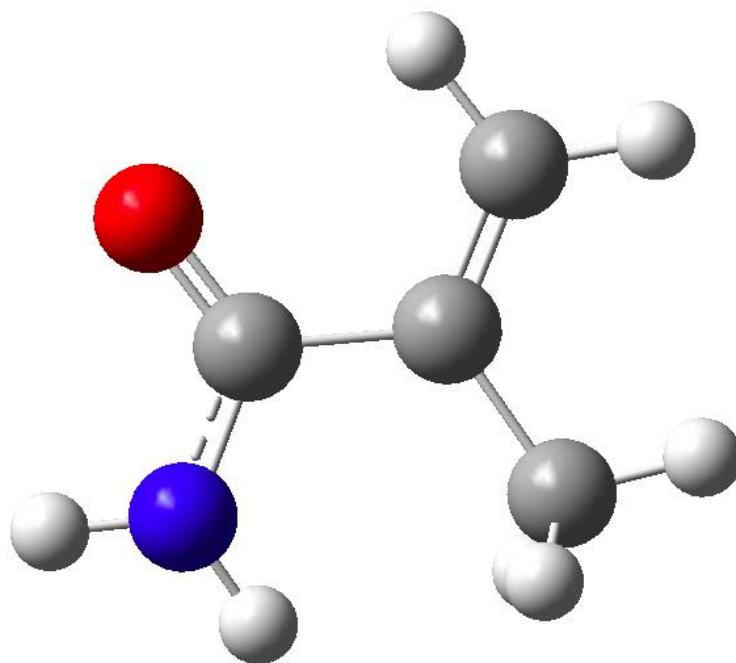


Figure 2.2.15 Structure A from energy diagram in Figure 2.2.14, $X = 1.30^\circ$, Energy = 1.2 KJ/mole

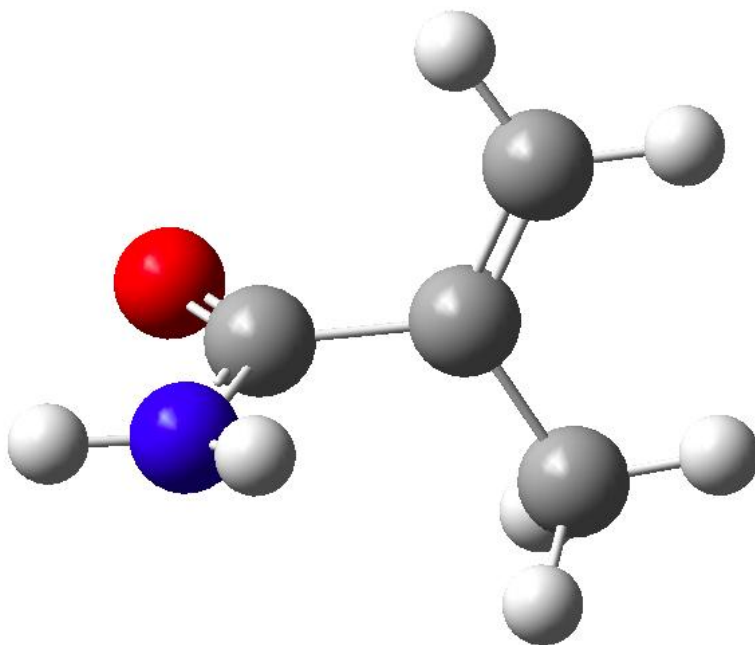


Figure 2.2.16 Structure B from energy diagram in Figure 2.2.14, $X = 81.30^\circ$ Energy = 18.5 KJ/mole.

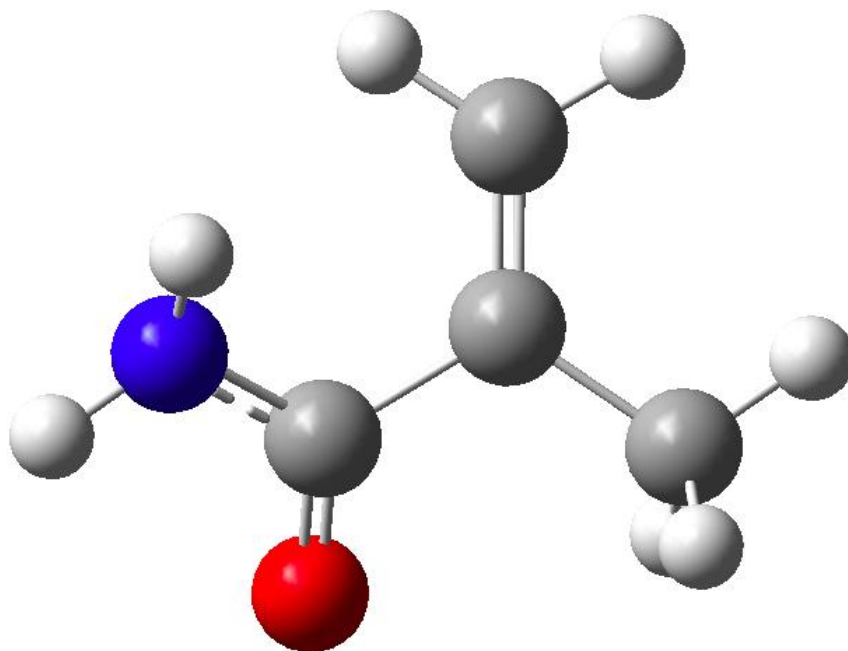


Figure 2.2.17 Structure C from energy diagram in Figure 2.2.14, X=151.30 °Energy = 0.0 KJ/mole.

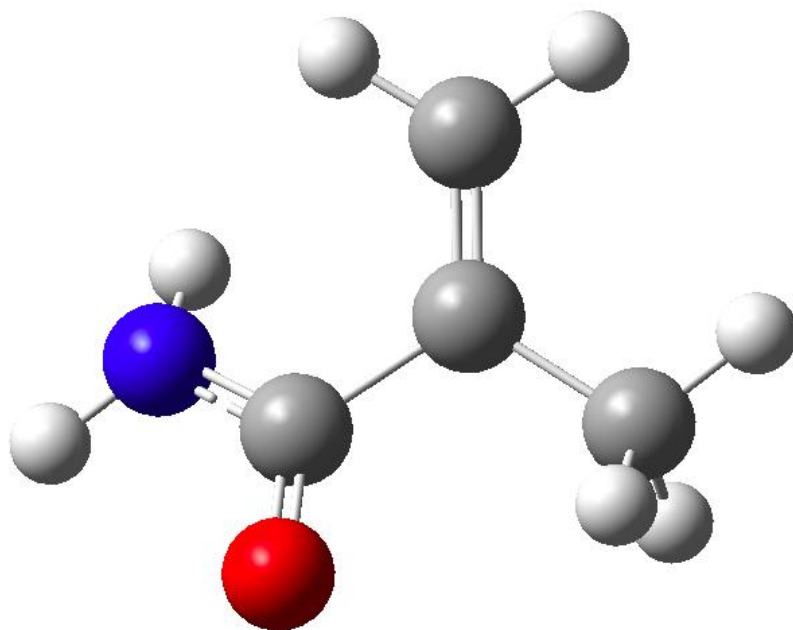


Figure 2.2.18 Structure D from energy diagram in Figure 2.2.14, $X = 211.30^\circ$ Energy = 0.0 KJ/mole.

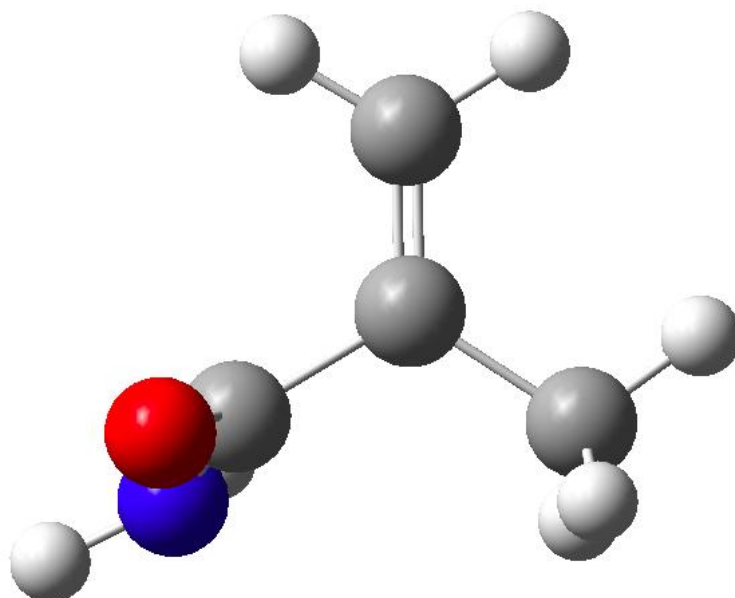


Figure 2.2.19 Structure E from energy diagram in Figure 2.2.14, $X = 281.30^\circ$ Energy = 18.6 KJ/mole.

The dihedral angle of O2-C1-C6-C8 = 0° was set as $X = 0^\circ$ and the energies were normalized to the lowest energy structure, Structure “E”, which had $X \approx 180^\circ$, potential energy = 0 KJ/mole. The potential energy of the $X = 1.30^\circ$ structure was 1.2 KJ/mole. The $X = 1.30^\circ$ structure (structure “A”) is the most stable. This conformation is referred to as the $X \approx 0^\circ$ structure. The energy difference between structure “A” and structures “C” or “D” was only 1.2 KJ/mole. That is, the difference between carboxamide geometries is much smaller in the propene model compound, than in the context of the pyridine ring of the nicotinamide.

The potential energy of the $X = 151.30^\circ$, $X = 180.0^\circ$, and $X = 211.30^\circ$ structures were 0.0 KJ/mole, 3.5 KJ/mole, and 0.0 KJ/mole respectively. Among these three structures, the $X = 151.30^\circ$ and $X = 211.30^\circ$ structures are the most stable (structures "C" and "D"). This conformation we call the $X \approx 180.0^\circ$ structure. Therefore, the most stable structures are Structures "C" and "D". But, in this propene derivative, the transition state barrier that must be traversed, in interconverting these structures, is higher than for the carboxamide attached to the pyridine group (Figures 2.2.1 and 2.2.7).

As before, there is steric hindrance between Hydrogen the thecarboxamide amide nitrogen (N3) in the amide group and the hydrogen attached to carbon C7 (also to C8, in the other conformation). The actual distance between hydrogens is below 2.56769 Å. Therefore, the $X = 0^\circ$ structure is not as stable a conformation compared to the other two structures: $X = -25.56^\circ$ and $X = 24.44^\circ$.

The distance between the hydrogen on the methyl and the hydrogen on the amide was 2.21707 Å. Therefore, there is no steric hindrance.

STUDIES OF REDUCED NICOTINAMIDE RING

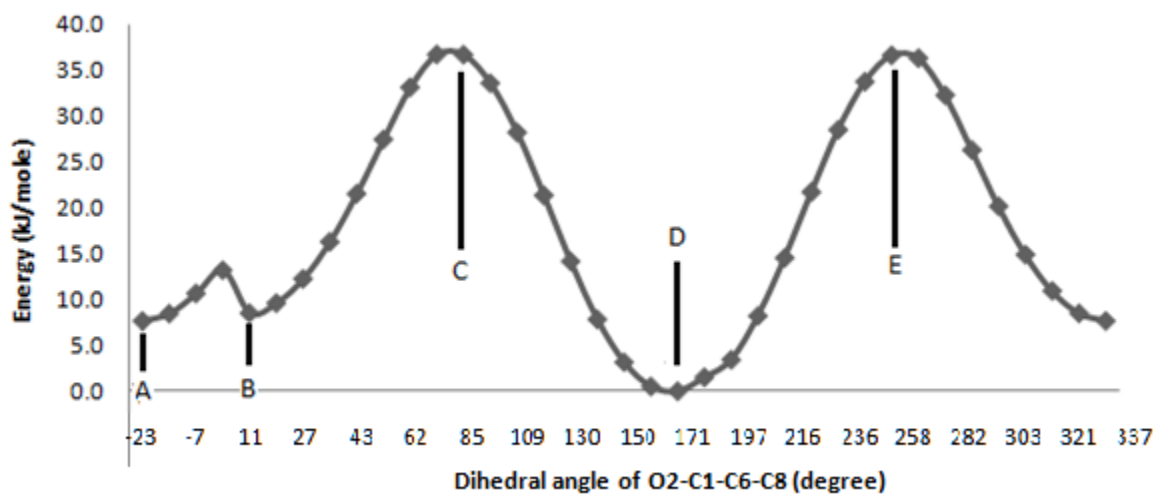


Figure 2.2.20 **Rotational Energy of C1-C6 bond in Reduced Nicotinamide**, X= 0 °is Dihedral angle of O2-C1-C6-C8 =0 °, Structure “A” was geometry optimized.

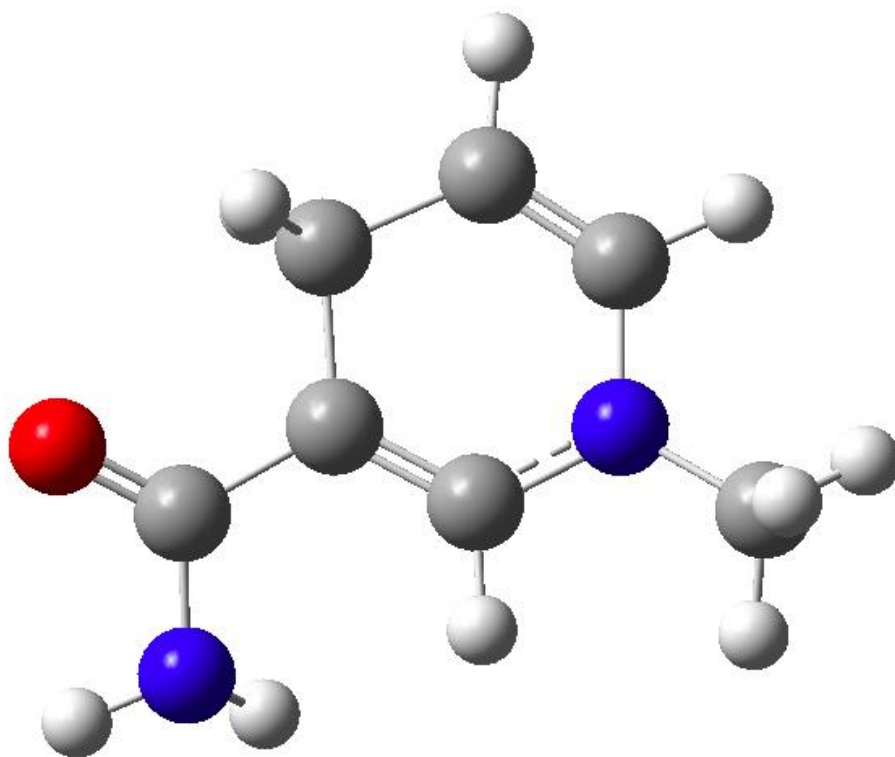


Figure 2.2.21 Structure A from energy diagram in Figure 2.2.20, X= -15.58 °Energy = 7.6 KJ/mole.

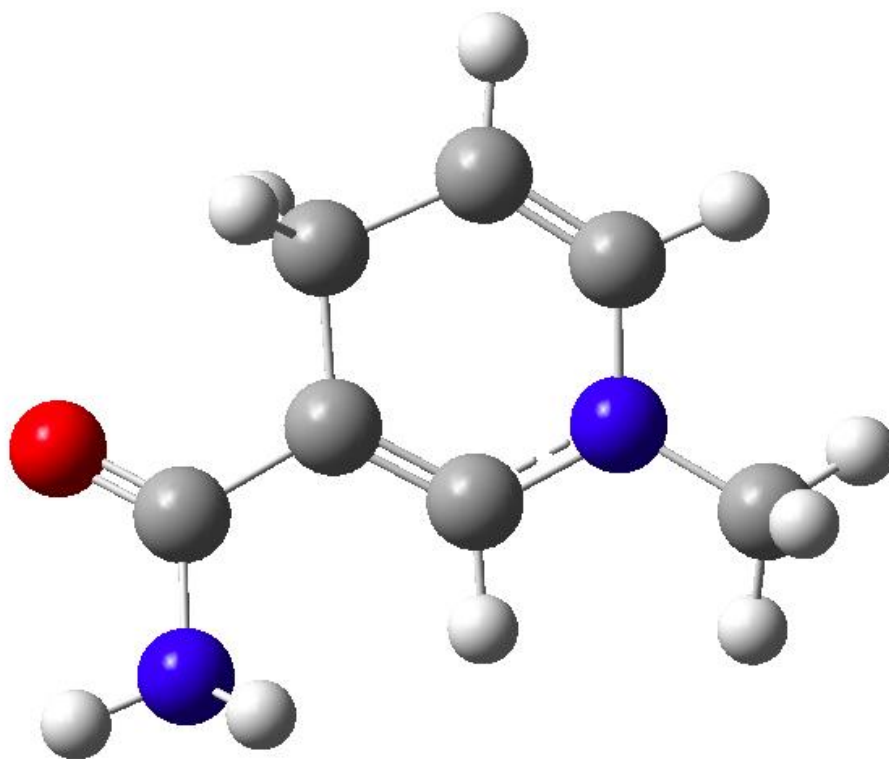


Figure 2.2.22 Structure B from energy diagram in Figure 2.2.20, $X = 15.37^\circ$ Energy = 8.5 KJ/mole.

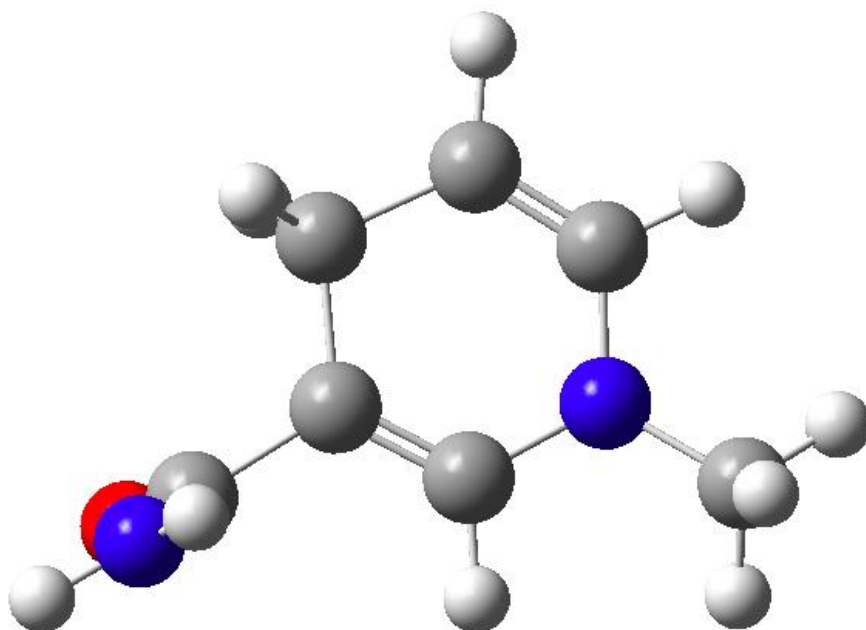


Figure 2.2.23 Structure C from energy diagram in Figure 2.2.20, $X = 81.86^\circ$ Energy = 36.7 KJ/mole.

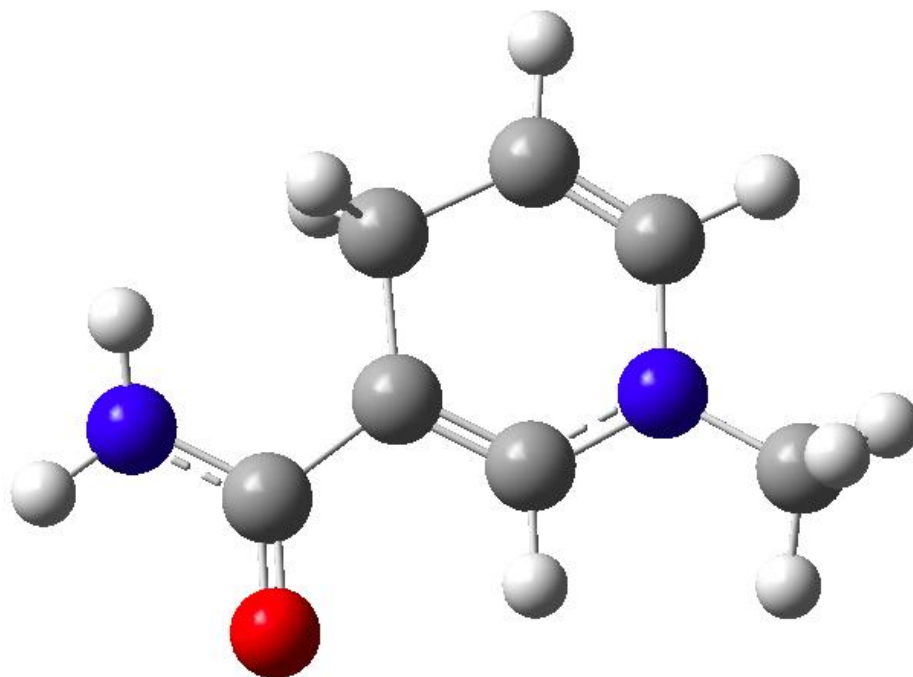


Figure 2.2.24 Structure D from energy diagram in Figure 2.2.20, $X = 179.18^\circ$ Energy = 0.0 KJ/mole.

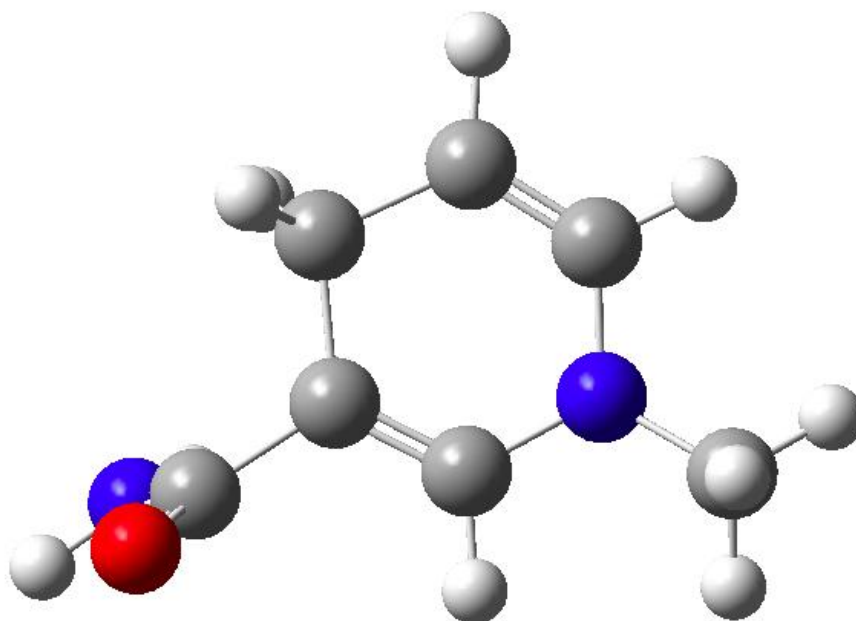
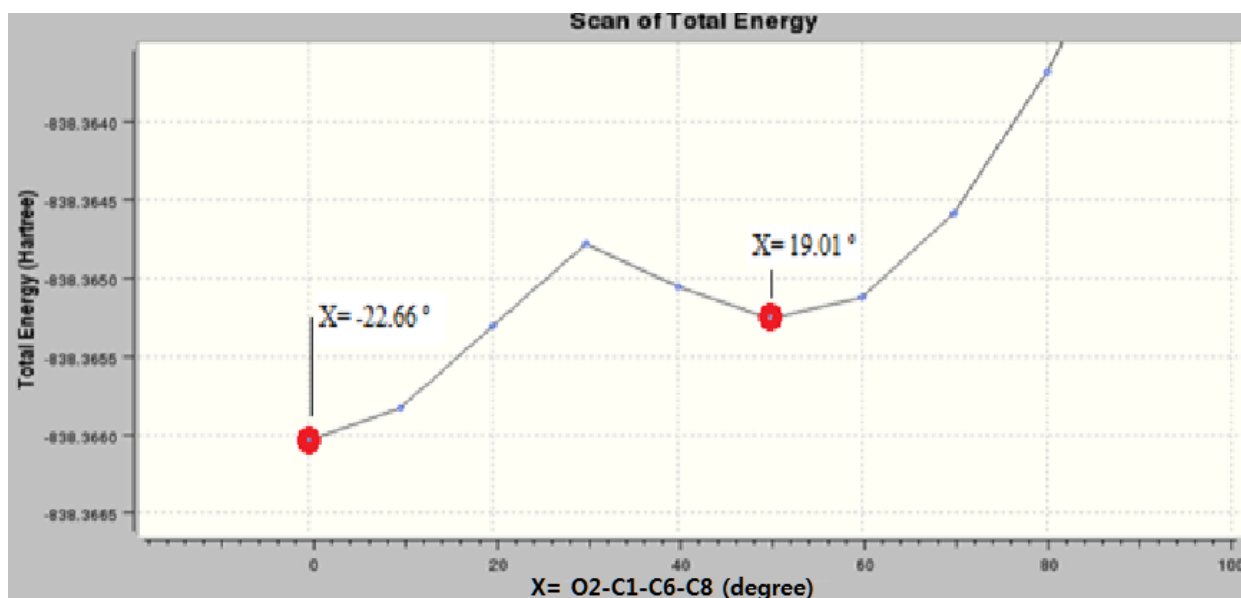


Figure 2.2.25 Structure E from energy diagram in Figure 2.2.20, $X = 260.75^\circ$ Energy = 36.6 KJ/mole.

The dihedral angle of O2-C1-C6-C8 = 0° was set as $X = 0^\circ$ and the energies were normalized to the lowest energy structure, Structure “D”, which had $X \approx 180^\circ$, potential energy = 0 KJ/mole. The potential energies for the $X = -15.58^\circ$, $X = 0^\circ$, and $X = 15.37^\circ$ structures were 7.6 KJ/mole, 11.9 KJ/mole, and 8.5 KJ/mole respectively. Among these three structures, the $X = -15.58^\circ$ structure (structure “A”) is the most stable. This conformation we call the $X \approx 0^\circ$ structure. The energy difference between structures “A” and “D” is 7.6 KJ/mole, the same as

that calculated for the oxidized nicotinamide ring, and with the same geometric preference for the carboxamide group. In comparing results from the various studies, the energy difference favoring the experimentally observed preferred geometry for the carboxamide group is not affected by redox state for the nicotinamide ring (it is the same for pyridine and dihydropyridine forms), is slightly diminished in the native cofactor with the ribose ring present (5 kJ/mole). But, in a simple allylic system (propene), there is little energy difference between the two carboxamide geometries.

The potential energy of the $X = 179.2^\circ$ structure is 0.0 KJ/mole. $X = 179.2^\circ$, and this structure (structure "D") is the most stable. This conformation we call the $X \approx 180.0^\circ$ structure. Therefore, the most stable structure of Reduced Nicotinamide is Structure "D", which is consistent with the above calculations for related structures..



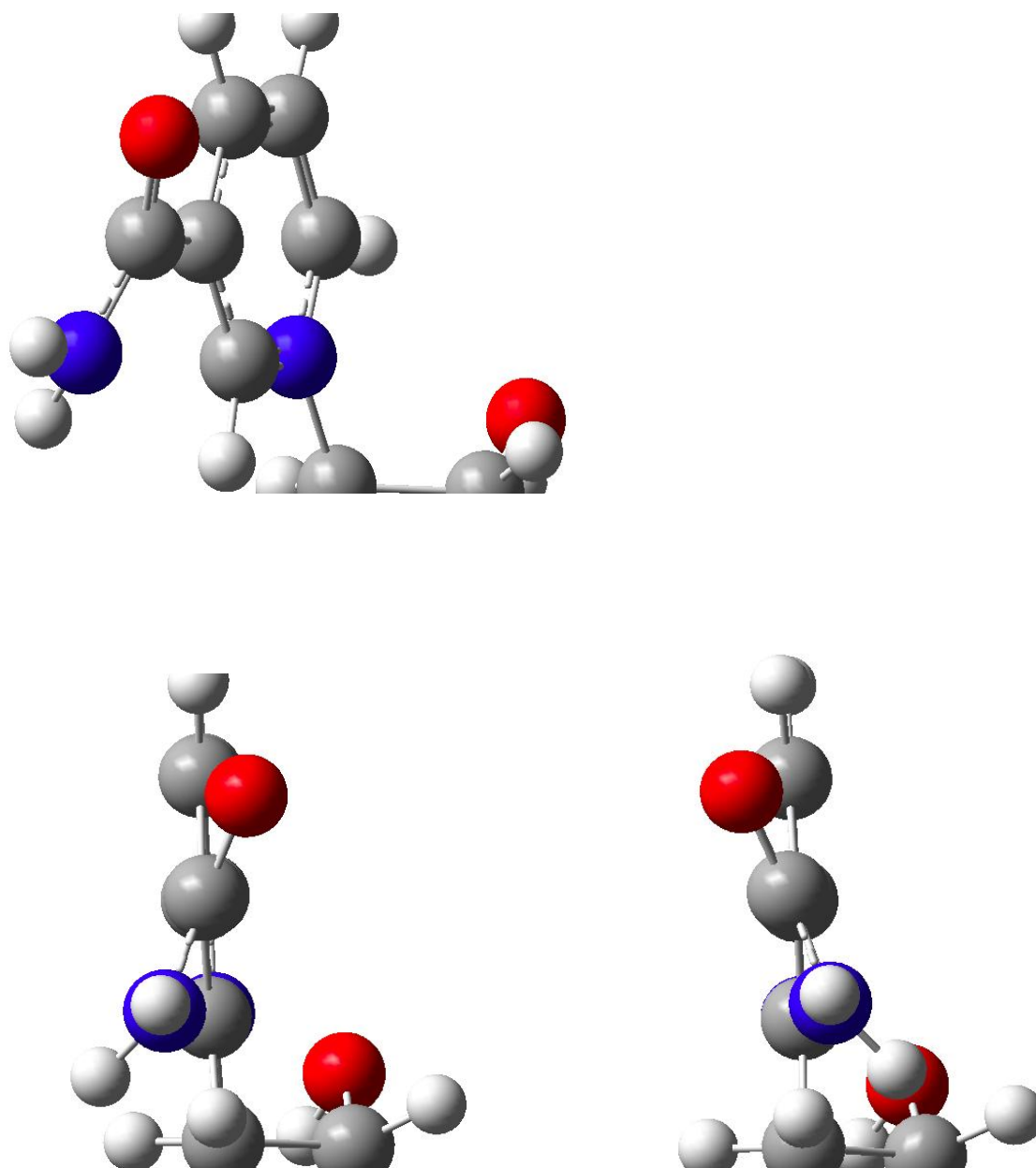


Figure 2.2.26 Top diagram: unbalanced energy diagram was taken from calculations used to generate Figure 2.2.1. Middle Figure: Snapshot from a portion of the Nicotinamide Nucleoside. Bottom Figure: left panel is for $X = -22.66^\circ$, Structure "A", and right panel is for $X = 19.01^\circ$, structure "B".

The Energy difference between structures A and B is not from steric hindrance between H4 on the amide and H9 and H11 on the pyridine in the Nicotinamide Nucleoside. The unbalanced W shape for the energy diagram (Figure 2.2.36, the middle Figure) came from the distortion of the pyridine structure. The shape of the pyridine for structures "A" and "F" is a boat shape (bigger distortion, Figure 2.2.28), which was presented previously by Cook, P. F.¹⁰³. The structures "C" and "E" are a somewhat distorted shape, close to planar. According to the Cook study¹⁰³, the boat conformation breaks the resonance on the Nicotinamide ring, so the Carboanion character Nicotinamide is localized at C-8 (Figure 2.2.27), making it susceptible to nucleophilic attack (and facilitating the hydride transfer reaction). The broken resonance structure "A", with the boat conformation, can be selectively stabilized in the enzyme active site to facilitate reaction.

The energy difference between the two carboxamide geometries ($X \sim 0$ or 180 degrees) in the Nicotinamide Nucleoside and Nicotinamide was 5.0 KJ/mole and 7.7 KJ/mole respectively. One important question is why the energy difference is smaller in Nicotinamide Nucleoside than in Nicotinamide; what effect is the ribose ring having? Ribose is acting as an electron withdrawing group which will weaken the resonance structure of Nicotinamide resonance structure. This supports the hypothesis that the structure in Nicotinamide Nucleoside is stabilized by resonance structures in pyridine ring.

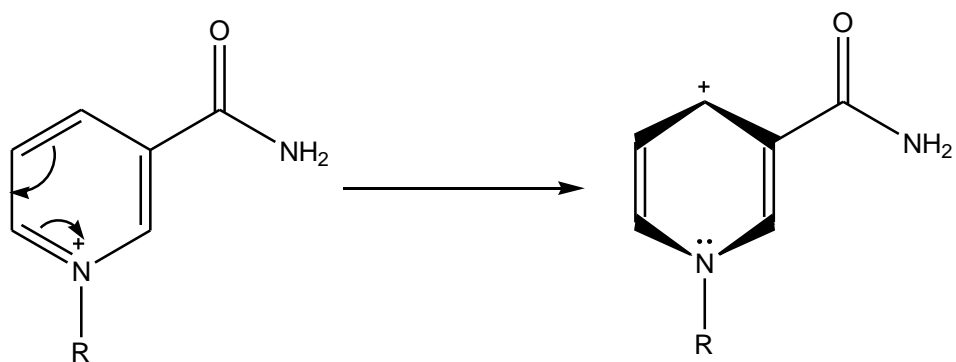
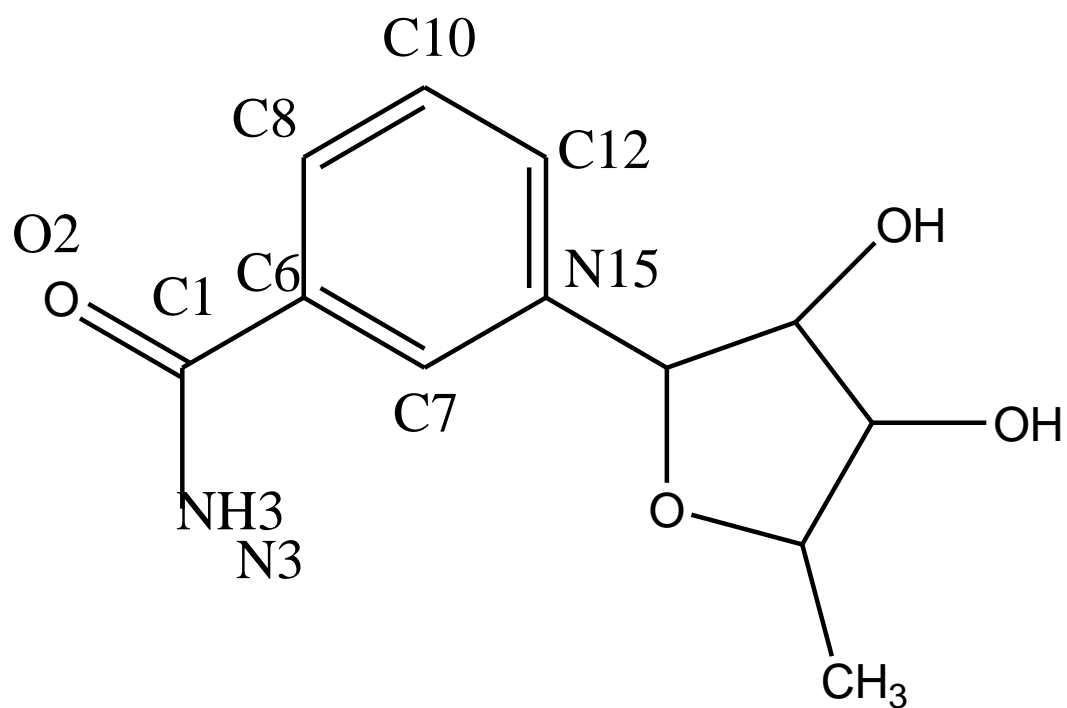
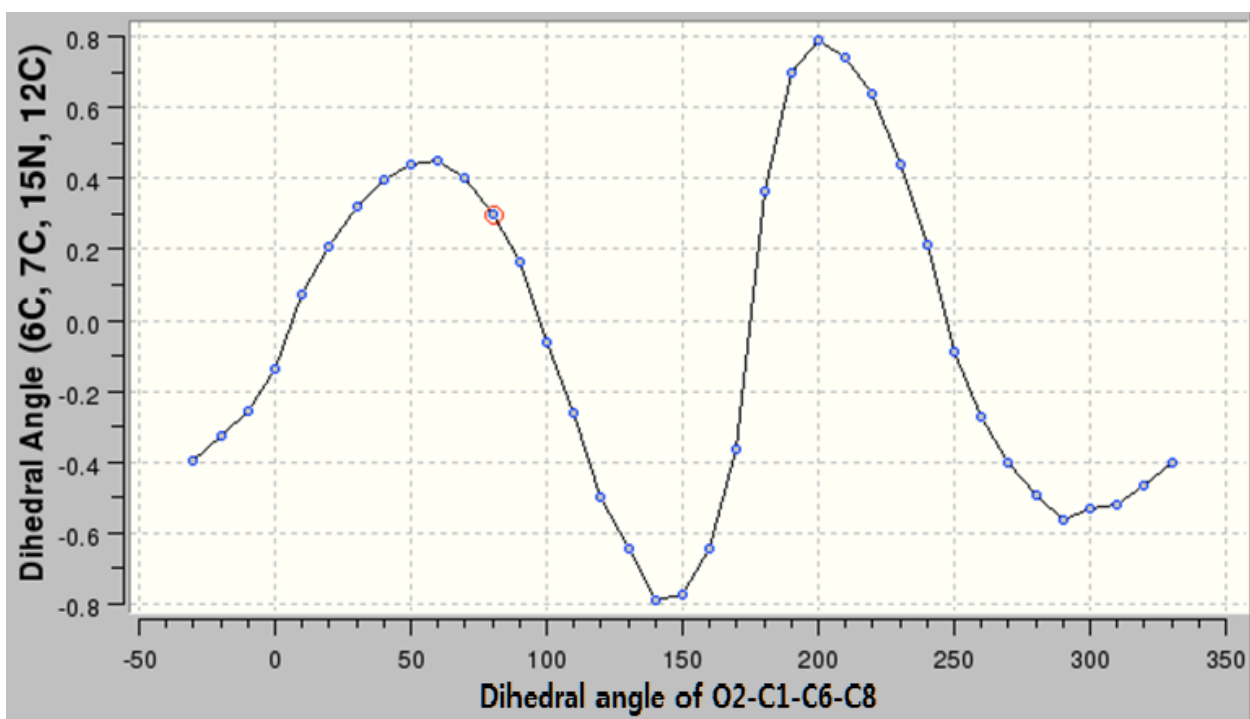
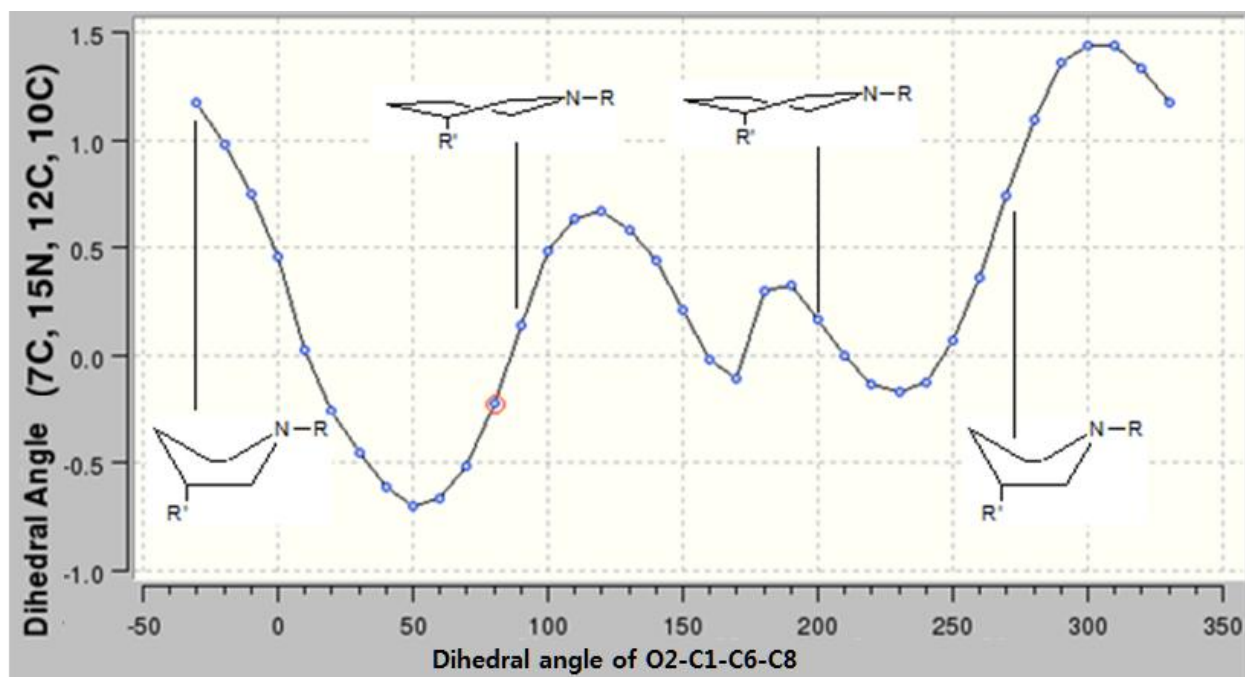


Figure 2.2.27 Resonance delocalization in the boat conformation





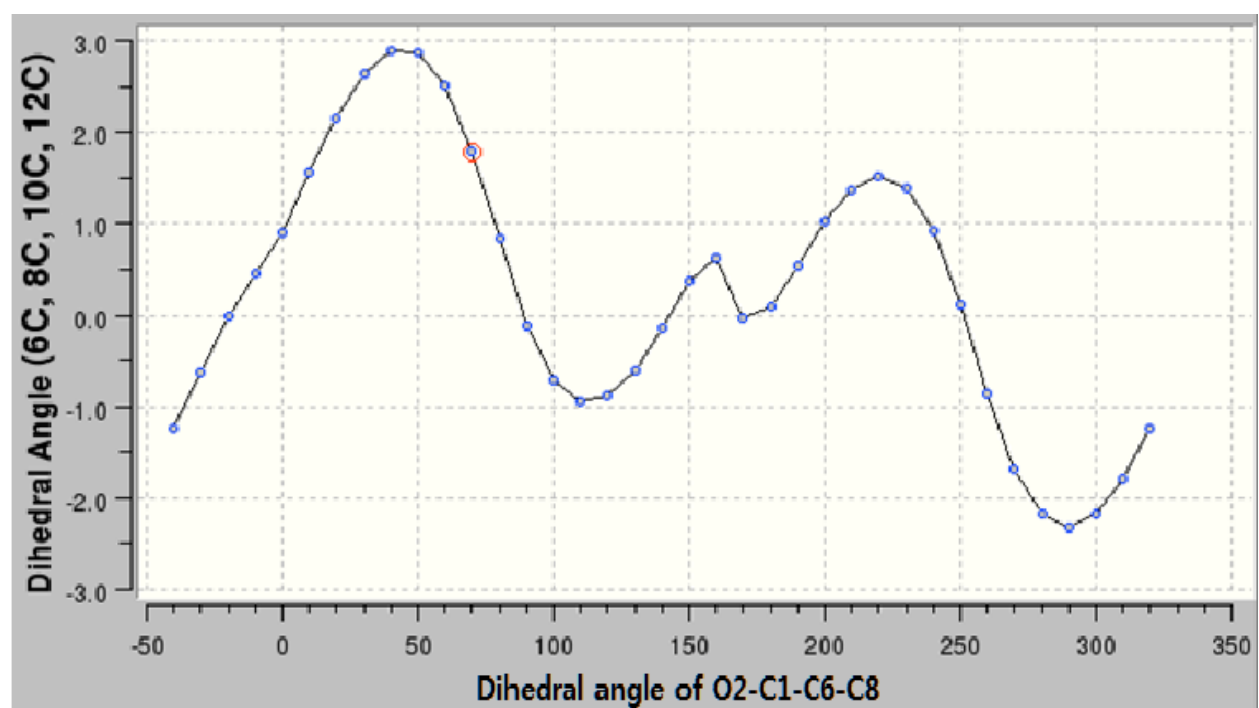
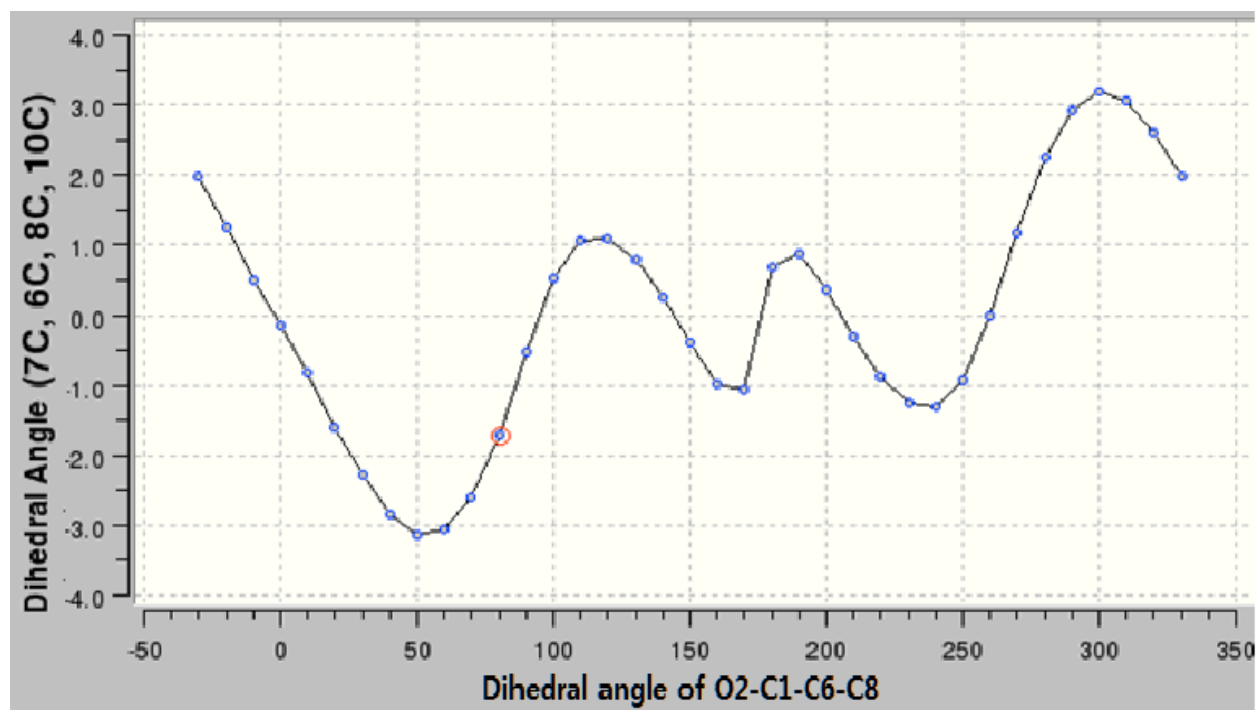


Figure 2.2.28 Dihedral angle of Pyridine in Nicotinamide Nucleoside. Using the above diagram, the shape of pyridine structure was drawn. Structure “A” has boat shape.

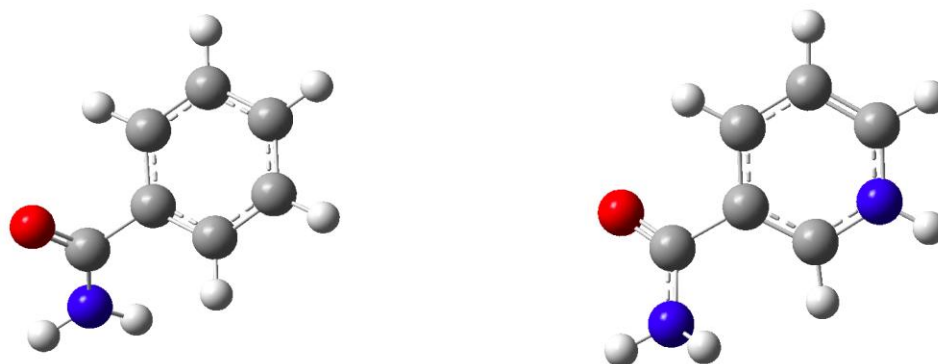
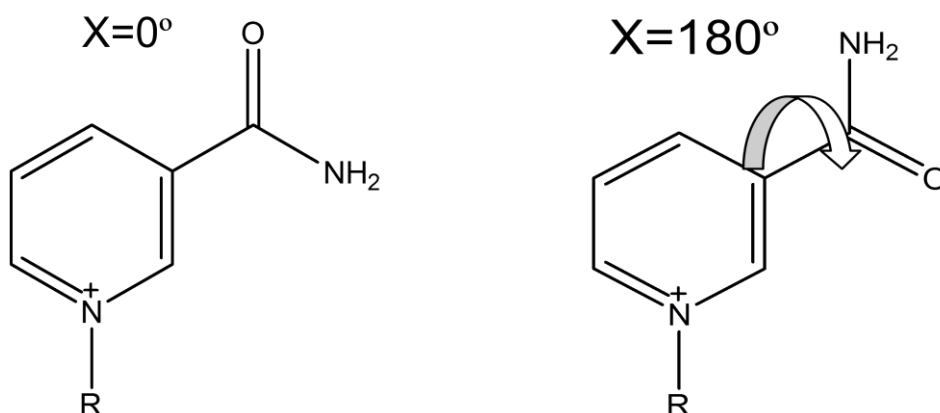


Figure 2.2.29 Energy calculation of Benzene (left) and Pyridine (right) substituent between $X \approx 0^\circ$ and $X \approx 180^\circ$ was calculated.

The geometrical optimizations of Benzene and Pyridine substituent which are showing in Figure 2.2.29 were performed. The Carboxamide group was rotated by 180° . The energy of two structures of Benzene and Pyridine substituent were compared. The benzene structure was same in Energy. However, the energy of pyridine substituent was different in 7.5 KJ/mole ($X \approx 0^\circ$ structure was less stable than $X \approx 180^\circ$).



	Nicotinamide Ribose	Nicotinamide	Pyridine Substituent	Benzene
-R group	Ribose	Methyl	Hydrogen	-
ΔE 0° vs 180° (KJ/mole)	5	7.7	7.5	0

Figure 2.2.30 Energy change after rotation of X

According to Figure 2.2.30, the substituent attached to N⁺ influenced the energy difference between $X \approx 0^\circ$ and $X \approx 180^\circ$. More electron withdrawing group such as Ribose reduced the energy difference between $X \approx 0^\circ$ and $X \approx 180^\circ$. The opposite effect was observed with electron donating group such as methyl. The oxygen on ribose can have interaction with hydrogen on hydrogen on carboxamide. This needs to be investigated further more.

2.3 Calculated charges on nicotinamide ring atoms of NAD(P)(H)

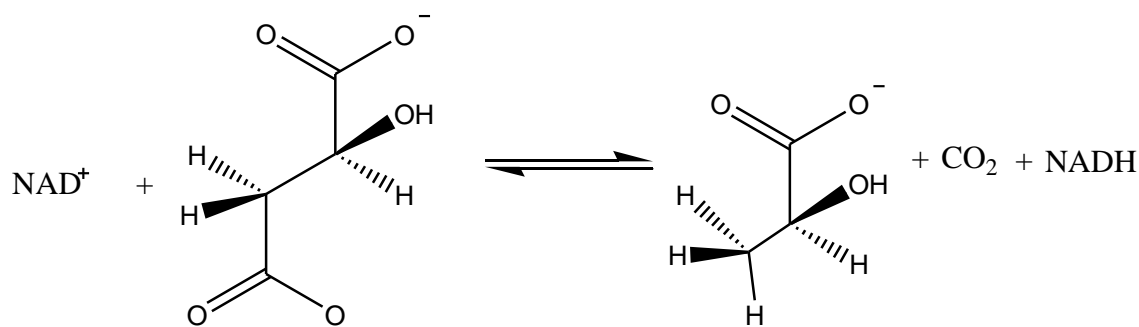


Figure 2.3.1 Malic Enzyme (ME) Reaction with the NAD⁺ Cofactor¹⁰¹

The NAD(P)⁺ cofactor is reduced to NAD(P)(H) by various oxidoreductase enzymes, including Malic Enzyme (Fig. 2.3.1). A hydride (proton and 2 electrons) is added to C8 of the nicotinamide ring (figure 2.3.2) in a reversible reaction. In general, oxidoreductase reactions involve hydride transfer to and from this position, and the transition state likely involves control of carbocationic character at this carbon, which may be tuned via enzymatic control of the pyridine ring geometry and interactions with the carboxamide group. An atomic charge analysis of NAD(P) will help the understanding of which factors play the most effective role in controlling this reaction.

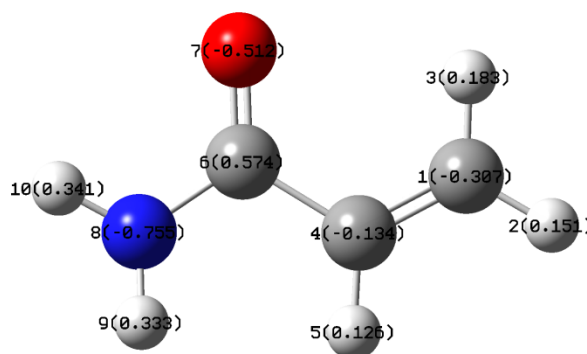
Calculation of charges (Table 2.3.1) supports the hypothesis that the Ribose is acting as an electron withdrawing group, which weakens resonance structures of the pyridine ring. The charge on C8 of the Nicotinamide Nucleoside and Nicotinamide was -0.177 and -0.069 at $X \approx 0^\circ$, which is generally more positively charged than for $X \approx 180^\circ$ (-0.19 and -0.099). While this is somewhat true for the oxidized nicotinamide, it is especially true for the reduced nicotinamide

where charge increases from -0.6 to -0.3. The Ribose affects charge on C8 as well, making it slightly less negative (weakly electron withdrawing, through resonance effects).

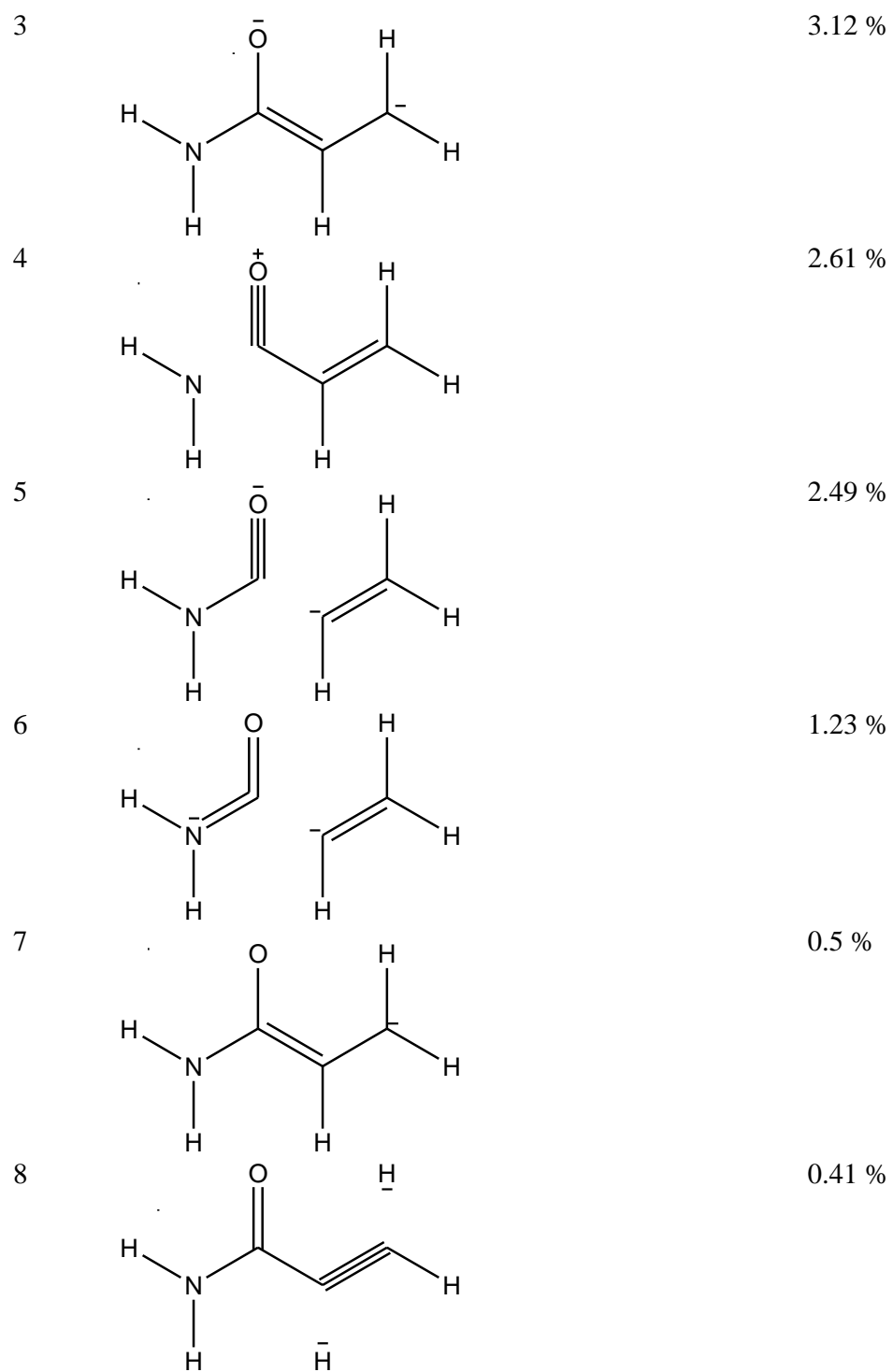
Name of molecule	X \approx 180 ° Oxidized N-N	X \approx 0 ° Oxidized N-N	X \approx 180 ° Oxidized N	X \approx 0 ° Oxidized N	X \approx 180 ° Reduced N	X \approx 0 ° Reduced N
C1	0.549	0.527	0.605	0.571	0.542	0.521
O2	-0.53	-0.501	-0.469	-0.442	-0.545	-0.512
N3	-0.768	-0.76	-0.758	-0.750	-0.768	-0.757
H4	0.335	0.329	0.359	0.351	0.33	0.317
H5	0.332	0.331	0.385	0.383	0.333	0.33
C6	0.002	0.01	0.013	0.014	0.01	0.004
C7	0.049	0.016	0.112	0.082	0.061	0.037
C8	-0.19	-0.177	-0.099	-0.069	-0.631	-0.322
H9	0.204	0.168	0.264	0.230	0.18	0.147
C10	-0.167	-0.169	-0.164	-0.165	-0.169	-0.171
H11	0.094	0.135	0.208	0.245	0.135	0.168
H11'	-	-	-	-	0.152	0.152
C12	0.009	0.006	0.119	0.121	0.079	0.068
H13	0.127	0.129	0.227	0.230	0.127	0.128
H14	0.164	0.165	0.239	0.239	0.141	0.138
N15	-0.473	-0.474	-0.387	-0.382	-0.431	-0.427

Table 2.3.1 Charge analysis* for Nicotinamide Nucleoside (N-N) and Nicotinamide (N)

2.4 Resonance structures for NAD(P)(H)



Entry	Resonance structure	Resonance Weight (%)
1		58.48 %
2		26.95 %



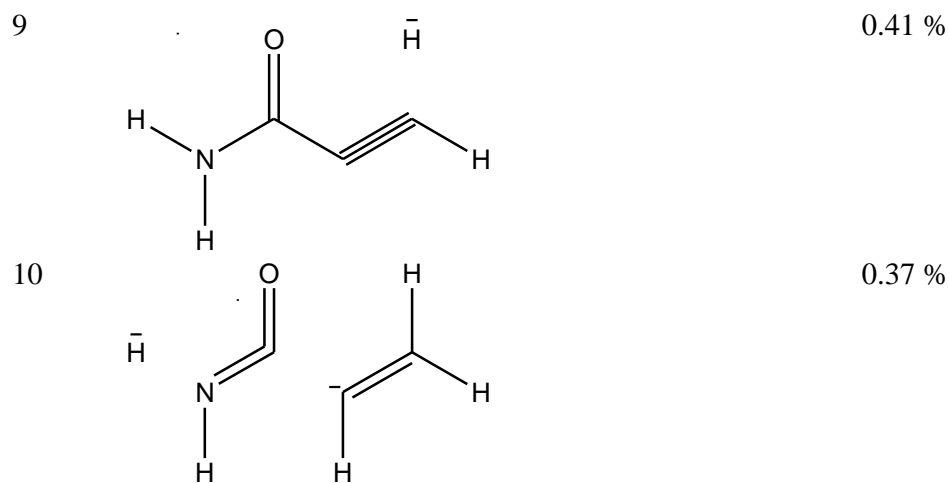
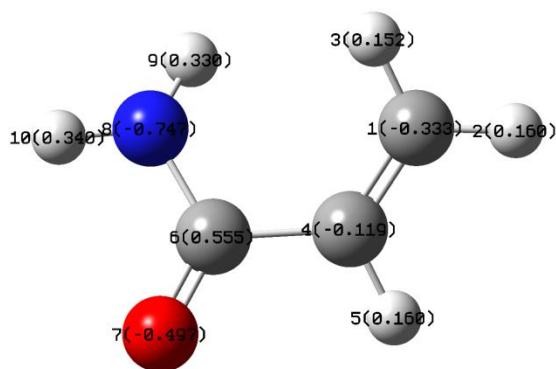
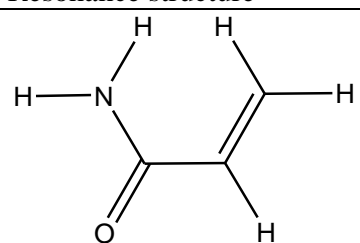
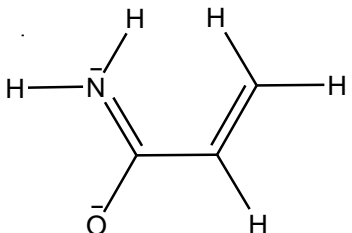
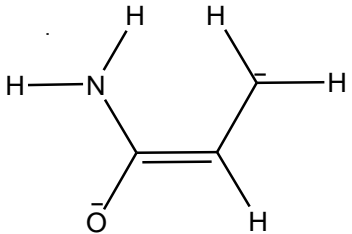
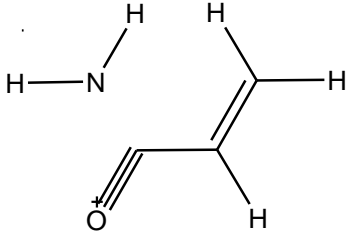
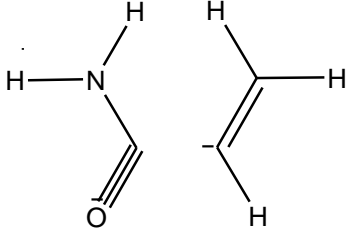
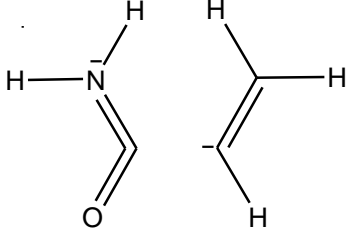
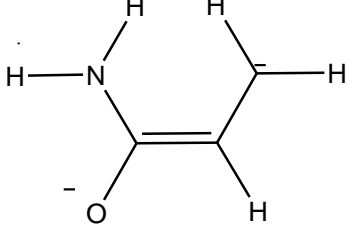


Figure 2.4.1 Resonance structure and weight of Acrylamide at $X \approx 0^\circ$



Entry	Resonance structure	Resonance Weight (%)
1		60.57 %

2		24.94 %
3		2.90 %
4		2.74 %
5		2.26 %
6		1.09 %
7		0.78 %

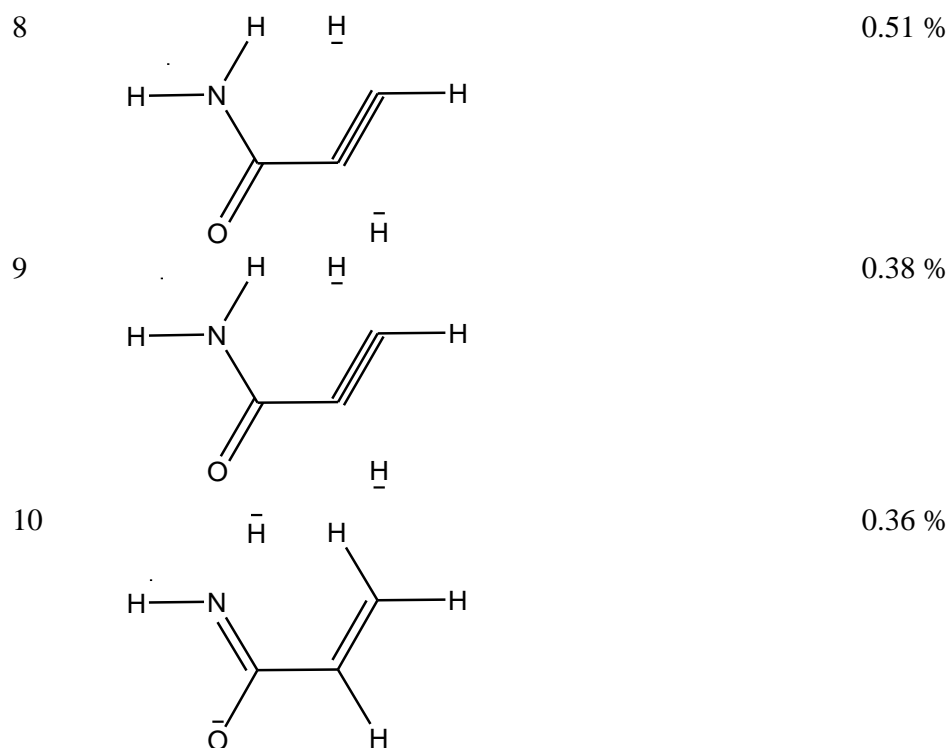
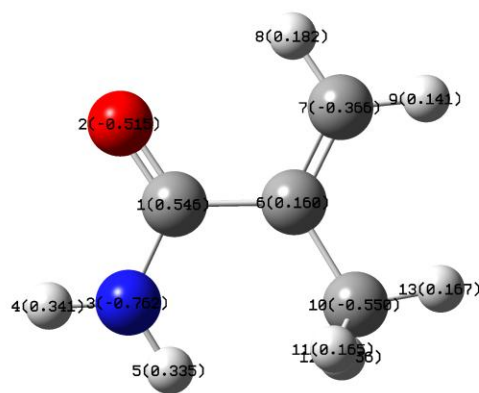
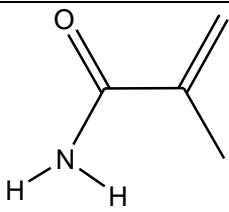
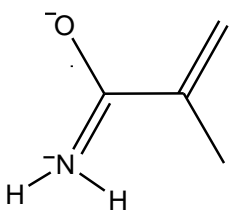
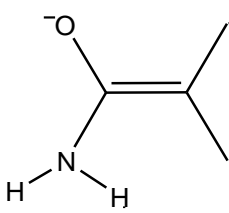
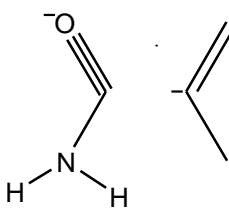
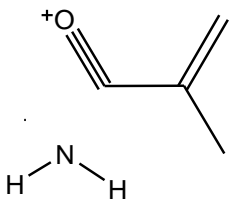
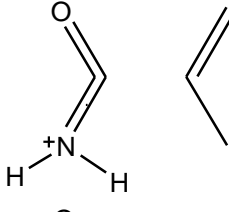
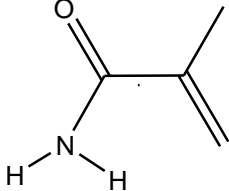


Figure 2.4.2 Resonance structure and weight of Acrylamide at $X \approx 180^\circ$



Entry	Resonance structure	Resonance Weight (%)
-------	---------------------	----------------------

1		56.19 %
2		26.10 %
3		2.66 %
4		2.54 %
5		2.53 %
6		1.27 %
7		0.61 %

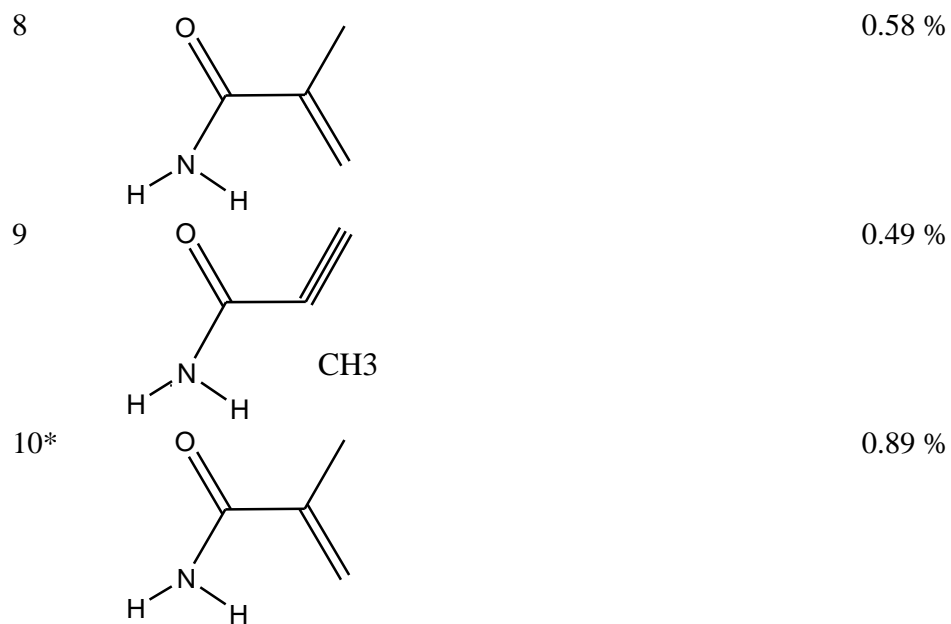
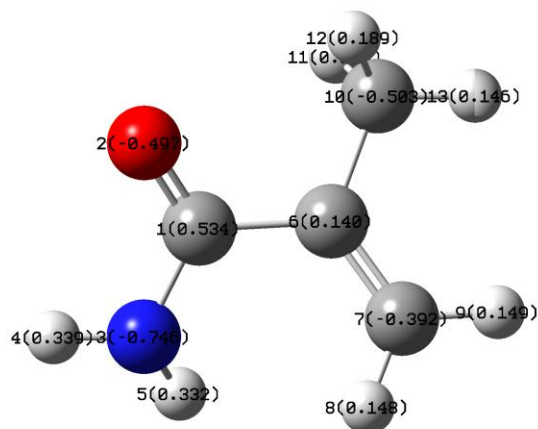


Figure 2.4.3 Resonance structure and weight of Methyl acrylamide at $X \approx 0^\circ$

*Structure 10: Total resonance weight of both H11 and H12 detached from C10



Entry	Resonance structure	Resonance Weight (%)
1		57.99 %
2		24.10 %
3		2.59 %
4		2.41 %

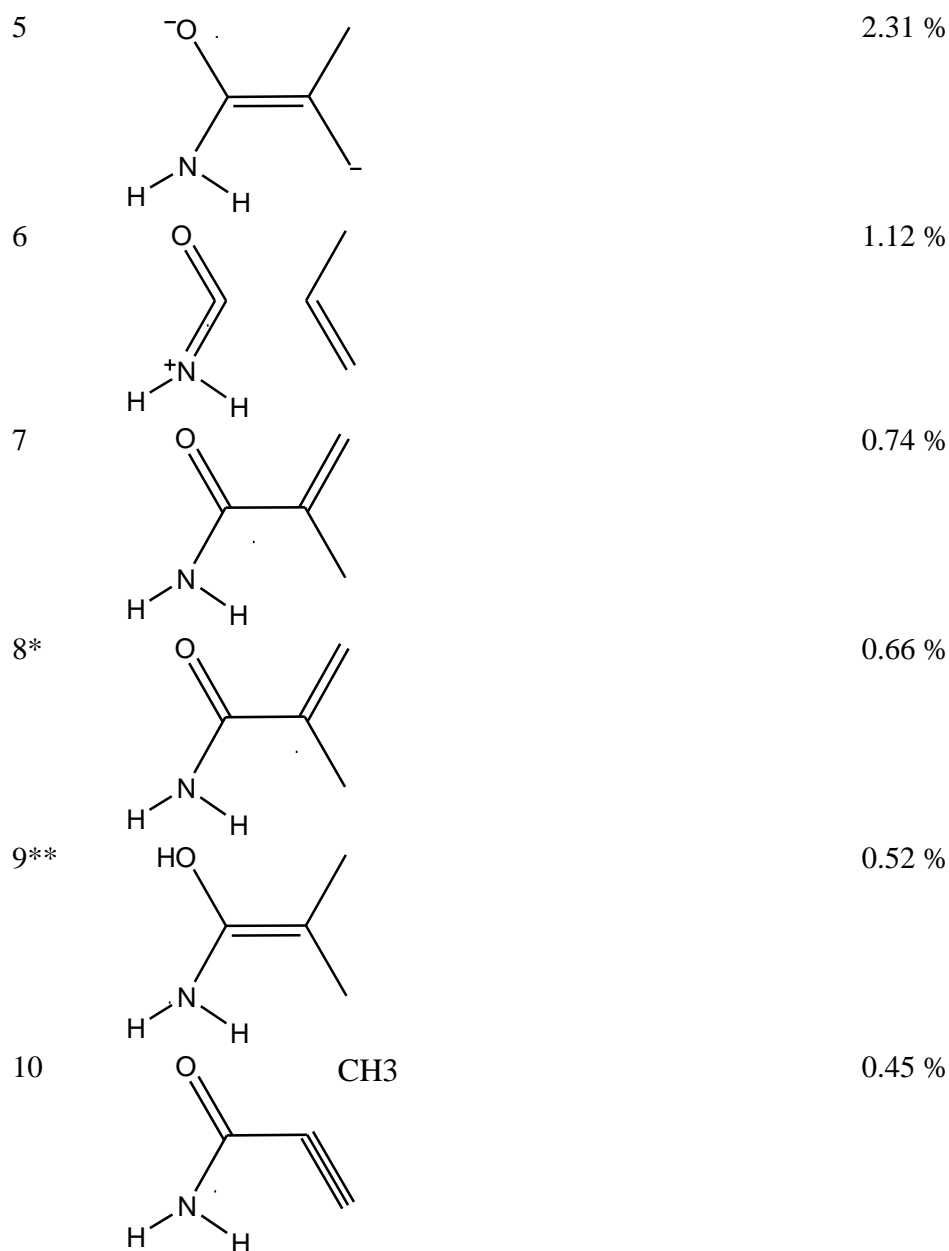


Figure 2.4.4 Resonance structure and weight of Methyl acrylamide at $X \approx 180^\circ$; structure 8*(H11 detached from C10); Structure 9**(H12 detached from C10)

NBO5 calculations (with assistance from Dr. Timeragazin) were used to determine the major contributing resonance structures for a model compound to represent the NAD(P)(H)cofactor. In order to analyze the $X \approx 0^\circ$ and $X \approx 180^\circ$ structures, the simplest model of NAD(P)(H) was used,

shown in Figures 2.4.1 and Figure 2.4.2 (Acrylamide) and Figure 2.4.3 and Figure 2.4.4 (Methacrylamide).

Figure 2.4.1 and Figure 2.4.3 summarize calculations for $X \approx 0^\circ$ and Figure 2.4.2 and Figure 2.4.4 for $X \approx 180^\circ$ structures. The NAD(P)(H) structure from figure 2.2.27 represents the target structure for this study, in terms of trying to better understand factors that stabilize reactive intermediates and transitions states in oxidoreductase hydride transfer reactions.

For Acrylamide, there is a 3.12 % contribution from one resonance structure of $X \approx 0^\circ$, which has a positive charge on Carbon 1 (Figure 2.4.1). Likewise, there is a 2.90% contribution from one resonance structure of $X \approx 180^\circ$, which has a positive charge on Carbon 1 (figure 2.4.2). So, the $X \approx 0^\circ$ structure produces more positive charge contribution on this carbon, as required by figure 2.2.27.

For Methacryamide, there is a 2.66 % contribution from one resonance structure of $X \approx 0^\circ$, which has a positive charge on Carbon 7 (Figure 2.4.3) which is C1 from (Figure 2.4.1).

Likewise, there is a 2.31% contribution from one resonance structure of $X \approx 180^\circ$, which has a positive charge on Carbon 7 (Figure 2.4.4) which is on Carbon 1 (figure 2.4.2). So, the $X \approx 0^\circ$ structure produces more positive charge contribution on this carbon, as required by figure 2.2.27.

2.5 Spectroscopic analysis of NAD(P)(H): calculation of NMR chemical shifts

The $X \approx 180^\circ$ and $X \approx 0^\circ$ structures of Nicotinamide Nucleoside and oxidized and reduced Nicotinamide were obtained from the rotational energy calculation. These structures were used for NMR chemical shift calculations (Figure 2.5.1) using Gaussian 9 with NMR=GIAO. Also, X

$\approx 180^\circ$ and $X \approx 0^\circ$ structures of Nicotinamide Nucleoside in air and in water solution were compared.

Calculated NMR chemical shifts of Oxidized Nicotinamide Nucleoside and Nicotinamide were compared. Hydrogen H4, H5, H9 and Nitrogen N3 were more shielded and shifted upfield in Nicotinamide (Table 2.5.2) compared to Nicotinamide Nucleoside, due presence of the Ribose, which is acting as an electron withdrawing group, taking electron density away from Pyridine ring in Nicotinamide Nucleoside and deshielding it. In particular, H9 in Pyridine was significantly deshielded.

H5 of Oxidized Nicotinamide Nucleoside and Nicotinamide was less shielded than H4. However, H5 of reduced Nicotinamide Nucleoside showed the opposite trend. H5 of reduced Nicotinamide Nucleoside was more shielded than H4. H5 of reduced Nicotinamide stays same, H5 of that is less shielded than H4 of that.

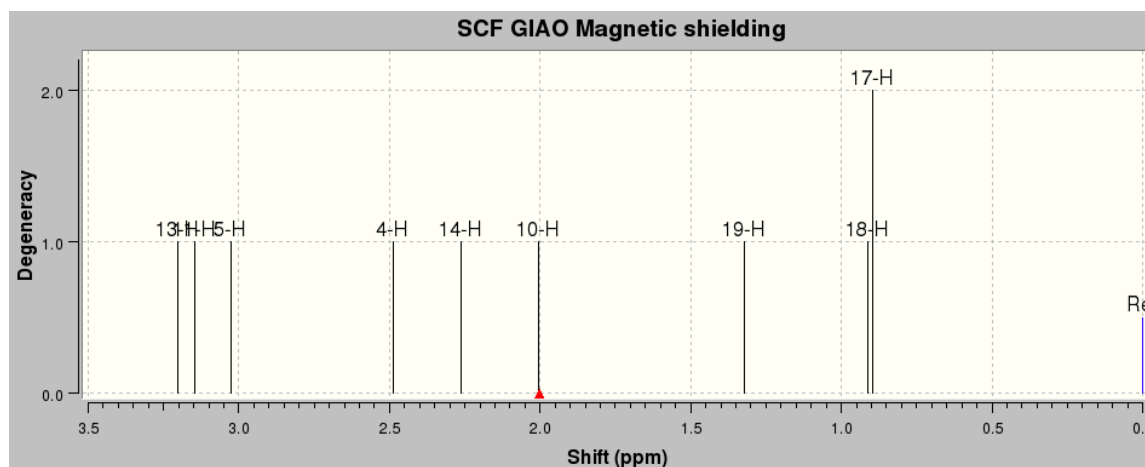


Figure 2.5.1 NMR chemical shift calculations for $X \approx 0$ and 180° structures of Oxidized Nicotinamide Nucleoside, Reference: TMS B3LYP/6-311+G(2d,p) GIAO

	H4	H5	N3	H9	*H9'
X \approx 0 °Oxidized Nicotinamide Nucleoside	4.4184	4.47658	94.4017	8.5492	
X \approx 180 °Oxidized Nicotinamide Nucleoside	4.77789	4.61491	94.4251	9.4132	
X \approx 0 °OxNicotinamide Nucleoside in water	4.4184	4.47658	94.4017	8.5492	
X \approx 180 °OxNicotinamide Nucleoside in water	4.77789	4.61491	94.4251	9.4132	
X \approx 0 °Oxidized Nicotinamide	4.5814	4.3463	94.656	8.9009	
X \approx 180 °Oxidized Nicotinamide	4.8669	4.7703	94.9359	7.8897	
X \approx 0 °Reduced Nicotinamide	2.7795	3.0324	85.9732	2.3808	2.9138
X \approx 180 °Reduced Nicotinamide	2.9816	3.2146	90.8374	2.6806	2.487

Table 2.5.2 Calculated NMR chemical shifts in ppm units. *H9', additional Hydrogen attached on C8 when NAD(P)⁺ is reduced. (See figure 1.5.1.)

2.6 Results and Discussion

Rotational energy calculations were performed for the carboxamide group in Nicotinamide Nucleoside, Nicotinamide, and the Propene-carboxamide, by rotating the carboxamide in 10 ° increments from 0 ° to 360 °. When the Dihedral angle of O2-C1-C6-C8 (Figure 2.2), X, is close to 0 ° or 180 °, the structure of the derivatives of NAD(P)(H) was stabilized, due to resonance contributions from the pyridine^{19,20}. But, the dihedral angle of O2-C1-C6-C8 positions the carboxamide out of plane, with the double bonds in the ring and strain of the Π -bonds being distorted and destabilized^{19,20}. The electron density of Nitrogen (N15) in Pyridine enhances Pyridine resonance structures with Π -bonds on one side more than that on the other side. This effect makes the structure of X=0 ° more stable than that of X = 180 °. The energy effect from this nitrogen was 7.7 KJ/mole in Nicotinamide.

In the studies presented herein, there was another question that arose. When the dihedral angle X is close to 0 ° or 180 °, there is an energy increase, a destabilization. This was caused by pyridine

ring distortions, involving steric clash between amide hydrogens and the pyridine ring¹⁹. The effect of these distortions were bigger than that of resonance stabilization in the $X=0^\circ$ or $X=180^\circ$ structures. The destabilization energy occurring in the pyridine ring, and causing distortion, was measured (Figure 2.2.1). The distortion energy in the $X=0^\circ$ structure is 2.9 KJ/mole, which was bigger than that in $X=180^\circ$ structure of 0.4KJ/mole. Therefore, the distortion in the $X=0^\circ$ structure was larger than that in $X=180^\circ$ structure by 2.5 KJ/mole.

This was confirmed with the pyridine structure analysis as had been proposed previously by Cook P. F. by dihedral angle calculations (Figure 2.2.28). The $X \approx 0^\circ$ structure was in a boat conformation, and was more distorted, with a dihedral angle range from 3.0° to -1.2° ; in contrast, the $X \approx 180^\circ$ structure was a distorted, but closer to planar, with a dihedral angle range from 0.4° to 0.0° .

The energy differences between $X \approx 0^\circ$ and $X \approx 180^\circ$ structures of Oxidized and Reduced Nicotinamide, and Oxidized Nicotinamide Nucleoside were 7.7 KJ/mole, 7.6 KJ/mole, and 5.0 KJ/mole respectively. The energy difference of Oxidized Nicotinamide Nucleoside was smaller than that of Nicotinamide by 2.7 KJ/mole. Ribose acted as an electronic withdrawing group, and destabilized the resonance structure of Pyridine - this is supported by Charge and NMR analysis. The effect of destabilization energy from an electronic withdrawing group, Ribose, is 2.7 KJ/mole.

The energy difference of Oxidized and Reduced Nicotinamide was insignificant, at 0.1 KJ/mole. The structural difference of these forms needs to be studied more deeply.

2.7 Conclusion

The energy effects of the carboxamide group rotation relative to the pyridine structure were dominated by four main factors: Resonance stabilization effect, Nitrogen electron withdrawing effect in the Pyridine ring, Distortion effect in the Pyridine ring due to H...H clashing, and Ribose ring effect.

Resonance stabilization effect was maximized when X is equal to 0° and 180° with $X \approx 180^\circ$ being more stable.

Nitrogen effect in Pyridine ring affects resonance stabilization energy difference (Different resonance weight on each side of pyridine ring) between $X \approx 0^\circ$ and $X \approx 180^\circ$ conformations, and is responsible in part for creating the preference for $X \approx 180^\circ$ via its electron withdrawal from the adjacent carbon.

Distortion effect in Pyridine ring destabilizes resonance stabilization effect.

Ribose ring weakens the Nitrogen electron withdrawing effect in the Pyridine ring, perhaps via electron donation due to the lone pair from oxygen. This could be proved by repeating calculations in the Anti orientation.

BIBLIOGRAPHY

APPENDIX

- (1) Salomon, J. A.; Lloyd-Smith, J. O.; Getz, W. M.; Resch, S.; Sanchez, M. S.; Porco, T. C.; Borgdorff, M. W. *PLoS Med.* **2006**, *3*, e273.
- (2) Zager, E. M.; McNerney, R. *BMC Infect. Dis.* **2008**, *8*, 10.
- (3) Lange, C.; Grobusch, M. P.; Wagner, D. *Dtsch. Med. Wochenschr.* **2008**, *133*, 374-376.
- (4) Reddy, S. G.; Sacchettini, J. C.; Blanchard, J. S. *Biochemistry* **1995**, *34*, 3492-3501.
- (5) Paiva, A. M.; Vanderwall, D. E.; Blanchard, J. S.; Kozarich, J. W.; Williamson, J. M.; Kelly, T. *M. Biochim. Biophys. Acta* **2001**, *1545*, 67-77.
- (6) Caplan, J. F.; Zheng, R.; Blanchard, J. S.; Vederas, J. C. *Org. Lett.* **2000**, *2*, 3857-3860.
- (7) Pavelka, M. S., Jr; Jacobs, W. R., Jr. *J. Bacteriol.* **1996**, *178*, 6496-6507.
- (8) Cirillo, J. D.; Weisbrod, T. R.; Banerjee, A.; Bloom, B. R.; Jacobs, W. R., Jr. *J. Bacteriol.* **1994**, *176*, 4424-4429.
- (9) Sidney P. C.; Nathana O. K.; Margaret M. C. *J. Biological chemistry.* 1951, ____, 447-459
- (10) Daniel S. Sem and Charles B. Kasper *Biochemistry* 1992. *31*. 3391-3398
- (11) Kwan-sa You *CRC Crit. Rev. Biochem.* 1985, *17*, 313
- (13) Oleg Jardetzky; Norma G. Wade Jardetzky, *J. Biol. Chem.* 1966, *241*, 85-91

- (14) Martin S. Pavelka JR. and William R. Jacobs, JR. *J. Bacteriol.* 1996, 178, 6496-9507
- (15) Cirillo, J. D; Weisbrod, T. R.; Banerjee, A; Bloom, B. R; Jacobs, W. R. Jr. *J. Bacteriol.* 1994, 176, 4424-4429
- (16) Chung J. L.; Ben G. H.; Paul F. C. *Archives of Biochemistry and Biophysics*, 1992, 299, 214-219
- (17) Sem D. S. et. al. *L. Chem. Biol.* 2004, 11. 185-194
- (18) David E.; Coleman G.S.; JagannathaRao E. J.; Paul F. C.; and Ben G. H., *Biochemistry*, 2002, 41, 6928-6938
- (19) Cook P. F.; Norman J.; Oppenheimer N. J.; Cleland W. W., *Biochemistry*, 2, 1817-1825, 1981
- (20) Kim K. B.; Jay S.S. *J. Am. Chem. Soc.*, 115, 10782-10785, 1993